Synthesis and Evaluation of ^{11}C-Labeled 6-Substituted 2-Arylbenzothiazoles as Amyloid Imaging Agents

Chester A. Mathis,*,† Yanming Wang,† Daniel P. Holt,† Guo-Feng Huang,† Manik L. Debnath,‡ and William E. Klunk‡

Departments of Radiology and Psychiatry, University of Pittsburgh, Pittsburgh, Pennsylvania 15213

Received January 16, 2003

The synthesis and evaluation of a series of neutral analogues of thioflavin-T (termed BTA's) with high affinities for aggregated amyloid and a wide range of lipophilicities are reported. Radiolabeling with high specific activity [^{11}C]methyl iodide provided derivatives for in vivo evaluation. Brain entry in control mice and baboons was high for nearly all of the analogues at early times after injection, but the clearance rate of radioactivity from brain tissue varied by more than 1 order of magnitude. Upon the basis of its rapid clearance from normal mouse and baboon brain tissues, [*N*-methyl-^{11}C]2-(4′-methylaminophenyl)-6-hydroxybenzothiazole (or [^{11}C]6-OH-BTA-1) was selected as the lead compound for further evaluation. The radiolabeled metabolites of [^{11}C]6-OH-BTA-1 were polar and did not enter brain. The binding affinities of [*N*-methyl-^{3}H]6-OH-BTA-1 for homogenates of postmortem AD frontal cortex and synthetic Aβ(1−40) fibrils were similar (K_d = 1.4 nM and 4.7 nM, respectively), but the ligand-to-Aβ peptide binding stoichiometry was ∼400-fold higher for AD brain than Aβ(1−40) fibrils. Staining of AD frontal cortex tissue sections with 6-OH-BTA-1 indicated the selective binding of the compound to amyloid plaques and cerebrovascular amyloid. The encouraging in vitro and in vivo properties of [^{11}C]6-OH-BTA-1 support the choice of this derivative for further evaluation in human subject studies of brain Aβ deposition.

Introduction

The presence and regional abundance of amyloid plaques and neurofibrillary tangles (NFTs) in human postmortem brain are the defining characteristics of Alzheimer's disease (AD).[1−3] Amyloid plaques are comprised principally of amyloid-beta (Aβ) peptide fibrils, while NFTs consist primarily of filaments of hyperphosphorylated tau protein. A validated biomarker of amyloid deposition in brain would likely prove useful to identify and follow individuals at risk for AD and to assist in the evaluation of new antiamyloid therapies currently under development.[4−8] A number of groups have worked to develop radiolabeled amyloid-specific imaging agents (Chart 1), but efforts have been limited by poor brain entry, high levels of nonspecific binding, or low levels of specific binding in brain regions known to contain high concentrations of Aβ. We reported that while Chrysamine G (CG) possessed high affinity for Aβ fibrils and plaques,[9] the penetration of an ^{125}I-labeled CG derivative into normal rat brain was low.[10] Similar results were reported using a ^{99m}Tc-labeled CG derivative.[11] Other more chemically distant analogues of CG composed of styrylbenzene salicylic acids, such as X-34 (Chart 1), provided similar results of high in vitro binding affinity to aggregated Aβ and low brain penetration in normal rodent brain.[12−14] Further modification of the structure by removing the carboxylic acid groups to provide MeO-X-04 resulted in improved brain entry, but not to the degree typically necessary to provide a good noninvasive positron emission tomography (PET) imaging agent.[13] To overcome the low brain penetration of the styrylbenzenes, we developed neutral carbon-11-labeled derivatives of thioflavin-T, termed BTA's, that displayed both high affinity for aggregated Aβ and provided the high brain entry necessary for PET imaging.[15,16] Kung and co-workers developed similar radioiodinated thioflavin-T derivatives as potential Aβ imaging agents for single photon emission computed tomography (SPECT), and several of these compounds (e.g., IBOX and IMPY) show promise for this purpose with high binding affinities for aggregated Aβ and good penetration in mouse brain.[17,18] Another neutral and highly lipophilic tracer, fluorine-18-labeled FDDNP, for binding both amyloid plaques and NFTs has recently been reported.[19,20] The absolute retention of [^{18}F]-FDDNP demonstrated by time-radioactivity curves in an AD patient showed cortical areas to exceed the reference region, the pons, by only 10−30% at late imaging times, indicating the need to develop improved Aβ agents with higher signal-to-background ratios for PET imaging.

We report here the systematic in vitro and in vivo evaluation of a series of neutral thioflavin-T derivatives, whose structures are shown in Figure 1. These compounds are potential PET amyloid imaging agents when radiolabeled with the 20.4 min half-life, positron-emitting radionuclide carbon-11. Our short-hand nomenclature of these 2-arylbenzothiazole (BTA) compounds has previously been described.[15] Briefly, the 6-position substituent (R_6) is written before "BTA" and the number of methyl groups on the 4′-amino group is written after

* To whom correspondence should be addressed: PET Facility, B-938 UPMC Presbyterian, 200 Lothrop Street, Pittsburgh, PA 15213-2582. Telephone: (412) 647−0736. Fax: (412) 647−0700. E-mail: mathisca@msx.upmc.edu.
† Department of Radiology.
‡ Department of Psychiatry.

10.1021/jm030026b CCC: $25.00
Published on Web 05/24/2003

Chart 1

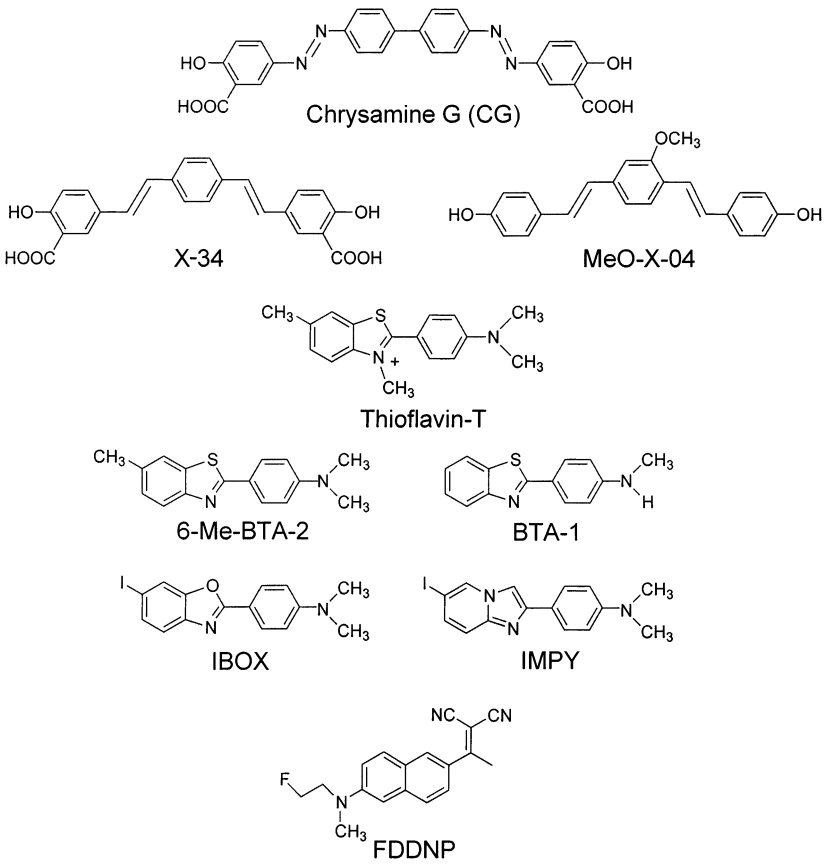

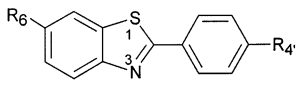

Figure 1. Structure of 6-substituted benzothiazole aniline (BTA) derivatives. Compounds reported here include the following: R_6 = H, CH_3, OCH_3, OH, CN, Br; $R_{4'}$ = NH_2, $NHCH_3$, $N(CH_3)_2$ (total of 18 BTA analogues).

"BTA". Thus 2-(4′-dimethylaminophenyl)-6-methylbenzothiazole, a compound with a 6-methyl group and a 4′-$N(CH_3)_2$ group, is referred to as "6-Me-BTA-2" (Chart 1).

Chemistry

Two different approaches were taken to synthesize the BTA precursors and standard compounds (Scheme 1). In approach A,[21] substituted anilines were transformed into *p*-nitrobenzoyl amides (**1** and **2**) and subsequently to the corresponding thioamides (**3** and **4**), which underwent cyclization to form 2-(4′-nitrophenyl)-benzothiazoles (**5** and **6**). Subsequent reduction of nitro group afforded 2-(4′-aminophenyl)benzothiazoles (**7** and **8**), from which compounds **9**−**14** were derived by methylation, demethylation, or aromatic substitution. In approach B, a series of 5-substituted *o*-aminothiophenols (**15**−**17**), which were prepared by base hydrolysis of the corresponding 2-amino-6-substituted-benzothiazoles,[22] were reacted with commercially available *p*-(methylamino)benzoic acid or (dimethylamino)benzaldehyde to form the secondary and tertiary amine derivatives, respectively. Thus, condensation of the 5-methoxy-substituted *o*-aminothiophenol with *p*-(methylamino)-benzoic acid in the presence of polyphosphoric acid[23,24] provided the secondary amine **18**, which was then selectively O-demethylated at the 6-position to afford **19**. Similarly, condensation of the 5-substituted *o*-aminothiophenols with *p*-(dimethylamino)benzaldehyde gave the tertiary amine compounds **20** and **21**. Approach A was more versatile than approach B, as a wide variety of substituted anilines were readily available. When a specific 2-amino-6-substituted benzothiazole was readily accessible, approach B was more straightforward, particularly for the synthesis of secondary amine derivatives as a result of the relatively low monomethylation yields of primary amines with methyl iodide.

Representative examples of ^{11}C-methylation conditions to produce a primary amine ([O-methyl-^{11}C]6-MeO-BTA-0; [^{11}C]**7**), a secondary amine ([*N*-methyl-^{11}C]6-OH-BTA-1; [^{11}C]**19**), and a tertiary amine ([*N*-methyl-^{11}C]6-MeO-BTA-2; [^{11}C]**18**) are described in the Experimental Section and shown in Scheme 2. Radiomethylation yields were higher for O-methylation (about 30% at end of synthesis (EOS)) compared to N-methylation (about 15% at EOS). This may be attributed to the fact that alkoxide group at the 6-position generated under basic conditions is a stronger nucleophile than the amino group at the 4′-position. It is worthwhile noting that no detectable [^{11}C]N-methylation was observed when 6-OH-BTA-0 was reacted with [^{11}C]methyl iodide (for about 10 min) in the presence of potassium carbonate, and only [O-methyl-^{11}C]6-MeO-BTA-0 was formed in relatively high yield. Thus, formation of [*N*-methyl-^{11}C]6-OH-BTA-1 required protection of the hydroxy group to block [^{11}C]O-methylation at the 6-position. The [^{11}C]N-methylated derivative was achieved in an overall modest yield following removal of the MOM-protecting group. For the [^{11}C]N-methylation of

Scheme 1. Synthesis of 6-Substituted 2-(4′-Aminophenyl)benzothiazoles

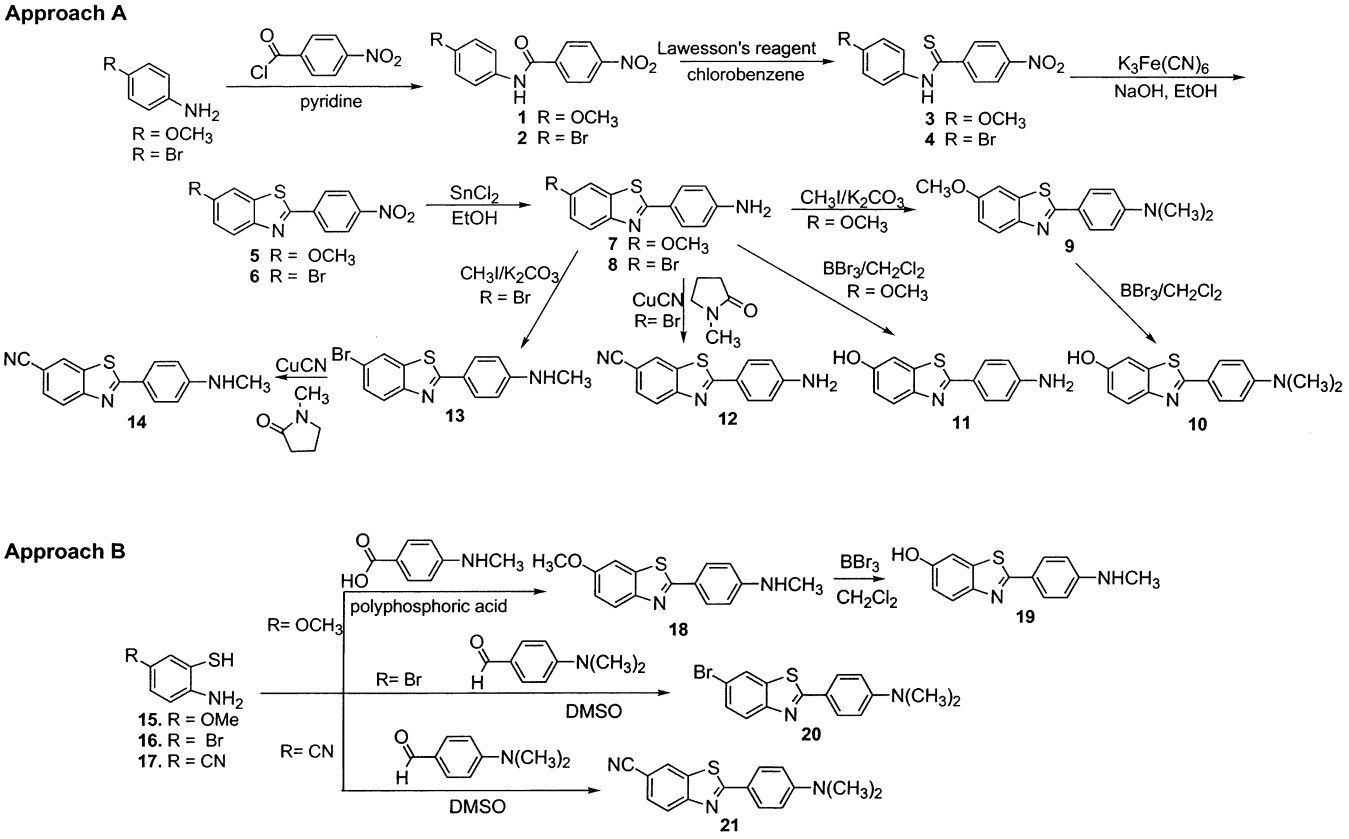

Scheme 2. Examples of Radiolabeling Reactions with [^{11}C]Methyl Iodide To Provide [*O*-Methyl-^{11}C]2-(4′-aminophenyl)-6-methoxybenzothiazole ([^{11}C]**7**), [*N*-Methyl-^{11}C]6-OH-BTA-1 ([^{11}C]**19**), and [*N*-Methyl-^{11}C]2-(4′-dimethylaminophenyl)-6-methoxybenzothiazole ([^{11}C]**9**). Also Shown Is the Synthesis of the MOM-Protected Precursor **24** for Subsequent Radiolabeling and Deprotection To Provide [^{11}C]**19**

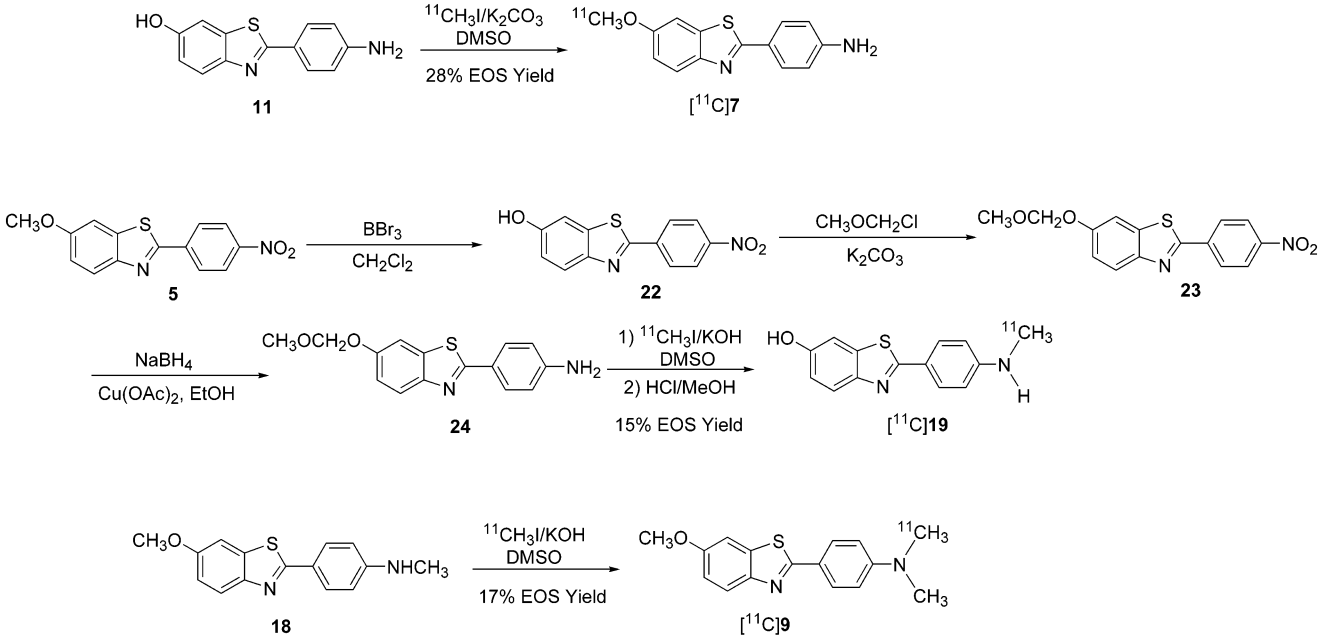

6-MOMO-BTA-0, the use of potassium hydroxide resulted in a considerably higher radiochemical yield than was achieved using potassium carbonate. However, relatively high N-methylation yields were achieved using potassium carbonate and nonradiolabeled (cold) methyl iodide for extended (16 h) reaction times at elevated temperatures.

Results

Table 1 shows the apparent lipophilicities (log P_{C18} values) of the eighteen BTA derivatives included in this study. For the four compounds in which the global lipophilicities (log P_{oct}) were determined by more standard shake-flask methods (shown in parentheses in

Table 1. Lipophilicity (log P_{C18}) and Aβ(1−40) Binding Affinities (K_i) of 6-Substituted BTA Analogues

	log P_{C18} R_4[a]			K_i (nM) $R_{4'}$		
R_6[a]	NH_2	$NHCH_3$	$N(CH_3)_2$	NH_2	$NHCH_3$	$N(CH_3)_2$
H	2.0	2.7 (2.7)[b,c]	3.4	37	11[c]	4.0
CH_3	2.4	3.1 (3.4)[b,c]	3.8	9.5	10[c]	64
OCH_3	1.9	2.6 (2.7)[b]	3.3	7.0	4.9	1.9
OH	0.66	1.2 (1.3)[b]	2.0	46	4.3	4.4
CN	1.8	2.5	3.2	64	8.6	11
Br	2.9	3.6	4.4	7.2	1.7	2.9

[a] R_6 and $R_{4'}$ refer to substituent positions shown in Figure 1. [b] The numbers in parentheses are log P_{oct} values determined by conventional octanol−buffer partitioning. [c] Previously published values shown here for comparison.[16]

Table 1), log P_{C18} correlated closely with log P_{oct} (r = 0.99). The log P_{C18} values of the BTA derivatives spanned and exceeded the log P_{oct} range of about 1−3 for compounds expected to enter the brain readily.[25,26] It should be noted that the log P_{C18} values for this group of BTA derivatives, relative to BTA-0, could be predicted fairly accurately using the substituent constants developed by Hansch and Leo.[27] For example, addition of an *N*-methyl group consistently increased the log P_{C18} by 0.7 units as predicted by Hansch substituent constants. The one notable exception was the effect of adding a hydroxyl group at the 6-position (R_6 in Figure 1). Instead of the expected decrease in log P_{C18} of 0.7 units, a decrease of ∼1.4 was consistently observed. This may be a result of the greater ionization of the phenol in these BTA compounds compared to the simpler phenols used by Hansch and Leo in determining their substituent constants. Using methods described by Klunk and co-workers,[15] the pK_a of the 6-OH-BTA-1 phenol was determined to be 9.3, while the pK_a of the (protonated) $^+NH_2CH_3$ group of 6-OH-BTA-1 was 3.0.

Table 1 also shows the binding affinities (K_i values) of the BTA derivatives for aggregated Aβ(1−40) fibrils in competition with [*N*-methyl-^{3}H]BTA-1. Affinities ranged from 1.7 to 64 nM, and all the BTA derivatives demonstrated much higher affinity for Aβ(1−40) fibrils than was previously observed for thioflavin-T (K_i = 580 nM).[16] Within a series with the same R_6 substituent, the more lipophilic secondary and tertiary amines were typically more potent than the primary amines. An exception to this trend was 6-CH_3-BTA-2 [$R_6 = CH_3$; $R_{4'} = N(CH_3)_2$], which appeared much less potent than predicted. This may be related to the fact that this very lipophilic compound (log P_{C18} = 3.8) was poorly soluble in the PBS buffer used for the binding assays.

Table 2 shows the brain entry of the BTA derivatives in Swiss-Webster mice in terms of percent injected dose per gram of brain (%ID/g) normalized to body weight (in kg) or (%ID-kg)/g. This latter unit can be directly compared across animals of very different size or across different species. Neuroreceptor radioligands that have been used successfully as PET tracers typically have (%ID-kg)/g values in the range of 0.1−0.5 within minutes after iv injection (e.g., refs 28−32). For mice whose body weight is about 30 g, this equals a brain concentration range of between 3.3 and 16.6%ID/g. All but two of the BTA derivatives were within this range at 2 min after injection. [^{11}C]BTA-1 showed the highest brain entry with a value of 0.43 (%ID-kg)/g. The highly lipophilic derivatives 6-Br-BTA-2 and 6-Me-BTA-2 showed the poorest brain entry, with (%ID-kg)/g values of only 0.054 and 0.078, respectively, and this may be a result of the phenomenon of blood element binding by highly lipophilic compounds (log P > 3).[25] The 2 min brain level of the BTA derivatives studied showed the classic parabolic relationship with log P_{C18} (Figure 2) described by Dishino and co-workers.[25] The only compound that appeared to not fit a parabolic-type relationship was [^{11}C]BTA-1, which demonstrated a considerably higher brain entry than any of the 12 other ^{11}C-labeled BTA derivatives.

Experiments to assess brain penetration of the radiolabeled derivatives were performed in young, wild type Swiss-Webster mice that had no amyloid deposits in their brain. Thus, this study reflects brain entry and clearance from normal brain tissue. A necessary criterion for a good PET imaging agent is rapid clearance from brain areas that do not contain the targeted binding site, particularly for relatively short-lived ^{11}C-labeled radioligands. The (%ID-kg)/g values of the BTA derivatives are shown in Table 2 and indicate that all but the two most lipophilic compounds, 6-Br-BTA-2 and 6-CH_3-BTA-2, provided lower 30 min brain values than 2 min values. The compound with the lowest 30 min brain (%ID-kg)/g value was [^{11}C]6-OH-BTA-1, with a more than 3-fold lower concentration than any other derivative. Another measure of clearance for the BTA derivatives is shown by the ratio of the 2 min-to-30 min (%ID-kg)/g values in Table 2. Judged by this measure, both [^{11}C]BTA-1 and [^{11}C]6-OH-BTA-1 stand out as particularly promising compounds, with [^{11}C]6-OH-BTA-1 demonstrating the highest 2 min-to-30 min brain radioactivity ratio. Interestingly, there was a significant correlation between log P_{C18} and the clearance as expressed by the 2 min-to-30 min ratio (r = 0.79). The least lipophilic compounds tended to clear from brain the fastest (Figure 2), while the most lipophilic compounds accumulated in brain over 30 min.

PET imaging studies in baboons were performed with five different ^{11}C-labeled BTA-1 derivatives including [^{11}C]BTA-1, [^{11}C]6-OH-BTA-1, [^{11}C]6-MeO-BTA-1, [^{11}C]6-CN-BTA-1, and [^{11}C]6-Me-BTA-1. All of these radiotracers were injected in two or more baboon PET imaging studies to demonstrate consistent findings. Figure 3

Table 2. Mouse Brain Entry and Clearance of 6-Substituted BTA Analogues

	(%ID-kg)/g in brain at 2 min $R_{4'}$			(%ID-kg)/g in brain at 30 min $R_{4'}$			ratio of 2 min/30 min $R_{4'}$		
R_6	NH_2	$NHCH_3$	$N(CH_3)_2$	NH_2	$NHCH_3$	$N(CH_3)_2$	NH_2	$NHCH_3$	$N(CH_3)_2$
H	−	0.43	0.19	−	0.057	0.078	−	7.6	2.5
CH_3	−	0.22	0.078	−	0.083	0.15	−	2.7	0.52
OCH_3	0.32	0.33	0.16	0.084	0.10	0.14	3.8	3.2	1.1
OH	−	0.21	0.32	−	0.018	0.10	−	12	3.0
CN	−	0.32	0.24	−	0.063	0.097	−	5.0	2.5
Br	−	0.12	0.054	−	0.12	0.11	−	1.0	0.49

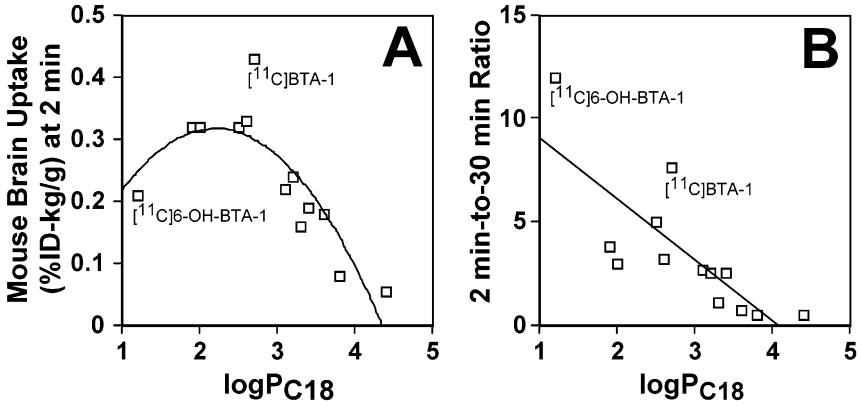

Figure 2. (A) Relationship between the brain entry of the ^{11}C-labeled BTA derivatives at 2 min after injection in control mice (Table 2) and the corresponding log P_{C18} value, a measure of the lipophilicity of the derivative (Table 1). (B) Relationship between the ratio of brain radioactivity concentrations ((%ID-kg)/g) at 2 and 30 min after injection (Table 2) and the lipophilicity of the ^{11}C-labeled BTA derivatives (Table 1).

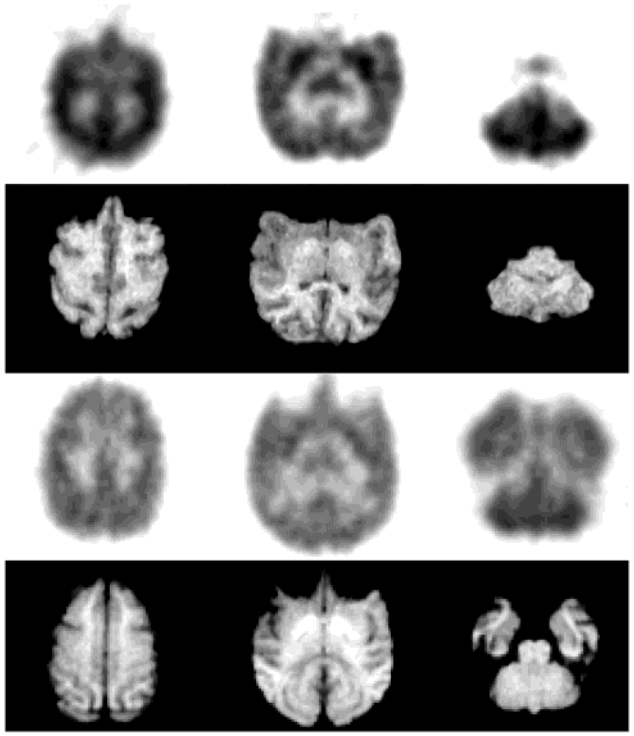

Figure 3. (top row) Summed PET images (0−9 min after injection) of the distribution of [^{11}C]BTA-1 in baboon brain at three different transverse levels. (second row) Coregistered SPGR MRI anatomical brain images of the same baboon. (third row) Summed images (0−9 min after injection) of the distribution of [^{11}C]6-OH-BTA-1 in baboon brain at three different levels. (bottom row) Coregistered SPGR MRI anatomical brain images of the same baboon.

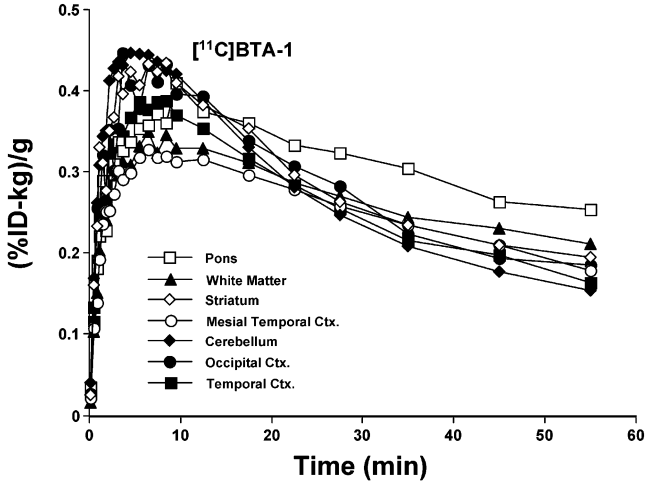

Figure 4. PET time−activity curves of the regional distribution of radioactivity in baboon brain following the injection of [^{11}C]BTA-1.

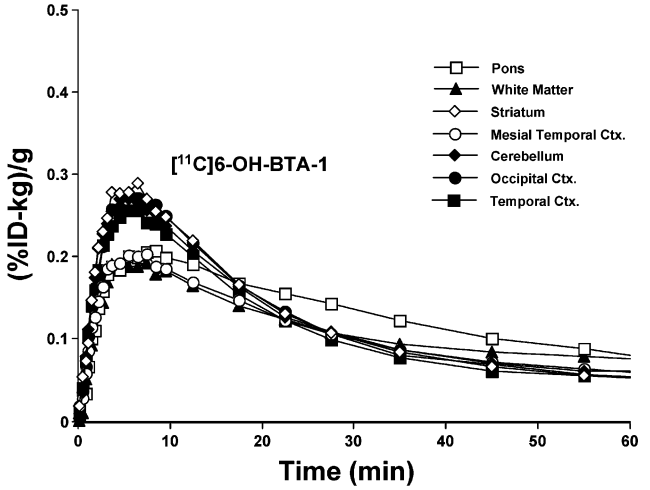

Figure 5. PET time−activity curves of the regional distribution of radioactivity in baboon brain following the injection of [^{11}C]6-OH-BTA-1.

shows typical early summed PET images (0−9 min after injection) in baboons for the two most promising derivatives from the mouse brain entry studies, [^{11}C]BTA-1 and [^{11}C]6-OH-BTA-1, with their corresponding coregistered MR images. At early time points, radioactivity appeared to be relatively uniformly distributed throughout the baboon brains, and these results were consistent with the expected absence of amyloid plaques in the brains of these control animals. However, time−activity plots of the regional concentration of radioactivity from 0 to 60 min indicated a heterogeneous distribution of brain radioactivity that was most apparent at later times (Figures 4 and 5). Regions of brain containing higher levels of white matter (such as pons) contained 20−30% higher concentrations of radioactivity at 60 min than regions that were dominated by gray matter such as temporal, mesial-temporal, and occipital cortex. The regional heterogeneity of radioactivity concentration was greater for [^{11}C]BTA-1 than for [^{11}C]6-OH-BTA-1,

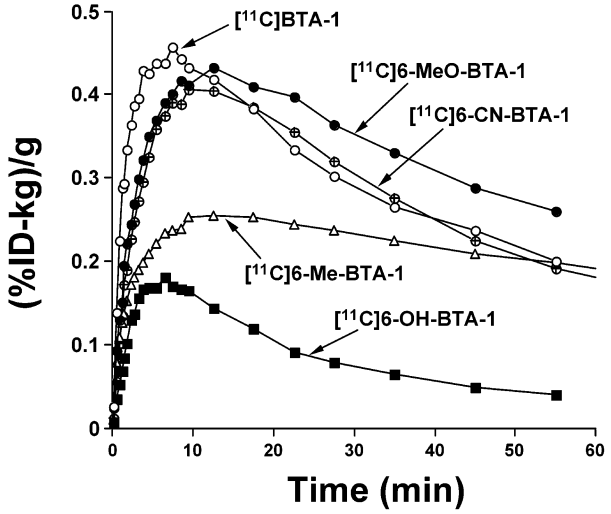

Figure 6. Comparison of the PET time-activity curves of radioactivity concentration in baboon cortex (summed over frontal, temporal, parietal, and occipital cortices) following the injection of five different ^{11}C-labeled BTA derivatives.

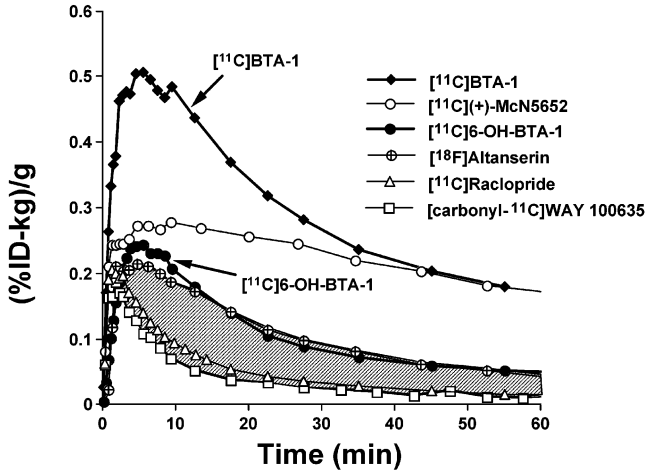

Figure 7. Comparison of the entry and clearance of radioactivity in baboon cerebellum of four reference PET radioligands ([^{11}C]raclopride, [carbonyl-^{11}C]WAY100635, [^{11}C](+)-McN5652, and [^{18}F]altanserin) relative to that for [^{11}C]BTA-1 and [^{11}C]6-OH-BTA-1. The shaded area is the desired target zone bounded by the cerebellar concentrations of the successful PET neuroreceptor radioligands [^{18}F]altanserin and [carbonyl-^{11}C]-WAY100635. [^{11}C]6-OH-BTA-1 demonstrated fairly rapid clearance of free and nonspecifically bound radioactivity from baboon cerebellum and was near the upper bound of the target zone, while [^{11}C]BTA-1 cleared relatively slowly from baboon cerebellum and was clearly out of the zone.

and the pons was particularly elevated for [^{11}C]BTA-1 as shown in Figure 4. The concentration of radioactivity in baboon cortex was nearly identical to that in the cerebellar cortex at all time points for all of the derivatives studied.

A comparison of typical time−activity curves for the ^{11}C-labeled BTA derivatives in the cortex of baboons is shown in Figure 6. The maximum brain radioactivity concentration (%ID-kg/g) in baboons correlated significantly with 2 min (%ID-kg)/g values in mice ($r = 0.85$), with the maximum brain concentration of radioactivity resulting from [^{11}C]BTA-1 > [^{11}C]6-MeO-BTA-1 > [^{11}C]6-CN-BTA-1 > [^{11}C]6-Me-BTA-1 > [^{11}C]6-OH-BTA-1. The brain radioactivity concentrations (%ID-kg/g) of [^{11}C]-BTA-1 and [^{11}C]6-OH-BTA-1 were remarkably similar in mice and baboons (0.43 vs 0.45 for [^{11}C]BTA-1 and 0.21 vs 0.27 for [^{11}C]6-OH-BTA-1). The rate of clearance of radioactivity was considerably slower from baboon brain than from mouse brain, although the rank order of clearance rate was similar in mice and baboons, with [^{11}C]6-OH-BTA-1 the fastest clearing and [^{11}C]6-Me-BTA-1 the slowest clearing derivative. Monoexponential fits of radioactivity loss from baboon cortices resulted in the following clearance half-times ($t_{1/2}$ values): [^{11}C]6-Me-BTA-1 = 111 min, [^{11}C]6-MeO-BTA-1 = 55 min, [^{11}C]6-CN-BTA-1 = 51 min, [^{11}C]BTA-1 = 20 min, [^{11}C]6-OH-BTA-1 = 13 min. As in the mice studies, [^{11}C]6-OH-BTA-1 and [^{11}C]BTA-1 resulted in the highest ratios of early-to-late brain radioactivity concentrations in baboons (4.6 and 2.8, respectively). Comparison of the in vivo behavior of the two lead compounds, [^{11}C]6-OH-BTA-1 and [^{11}C]BTA-1, in baboon brain to that of the entry and clearance of other successful PET radioligands in a reference brain region devoid of specific binding sites (i.e., cerebellum) was helpful in selecting the lead ^{11}C-labeled BTA derivative to take into human studies. The cerebellar time-activity curves in baboons of [^{11}C]raclopride, [carbonyl-^{11}C]WAY100635, [^{11}C](+)-McN5652, and [^{18}F]altanserin are compared to those of [^{11}C]6-OH-BTA-1 and [^{11}C]BTA-1 in Figure 7. The relatively rapid nonspecific binding clearance rates of [carbonyl-^{11}C]WAY100635, [^{11}C]raclopride, and [^{18}F]-altanserin are important in the success of these PET radioligands for imaging the serotonin 5-HT$_{1A}$, dopamine D$_2$, and serotonin 5-HT$_{2A}$ receptor systems.[33−38] In contrast, the relatively slow in vivo clearance of [^{11}C]-(+)-McN5652 has limited the usefulness of this radioligand for imaging the serotonin transporter system.[39,40] We reasoned that a ^{11}C-labeled BTA compound with similarly rapid nonspecific binding clearance properties within the range bracketed by [carbonyl-^{11}C]WAY100635 and [^{18}F]altanserin might prove useful as an in vivo imaging agent for amyloid plaques. The brain clearance properties of [^{11}C]6-OH-BTA-1 indicated that the relatively rapid rate of nonspecific clearance of this radiotracer ($t_{1/2}$ = 13 min) was similar to that of other useful PET neuroreceptor imaging agents and those of [^{11}C]BTA-1 ($t_{1/2}$ = 20 min) were too slow (Figure 7). Clearly, this comparison ignores the specific binding properties of the ^{11}C-labeled BTA derivatives, which could be as or more important than the rate of clearance of free and nonspecifically bound radioactivity from brain tissues,[41] and these in vivo specific binding studies are currently in progress. For this study, it was only possible to critically assess the rates of in vivo clearance of the free and nonspecifically bound radioactivity of the ^{11}C-labeled BTA derivatives in the brains of rodent and nonhuman primate animal models.

Because of the promising properties of [^{11}C]6-OH-BTA-1 in the brains of control mice and baboons, we further evaluated its in vivo and in vitro properties and compared them to those previously reported for [^{11}C]-BTA-1.[16] Scatchard analysis of [*N*-methyl-^{3}H]6-OH-BTA-1 binding to aggregated Aβ(1−40) fibrils showed a single binding component (Figure 8A) having a K_d of 4.7 nM and a B_{max} of 2.7 pmol of 6-OH-BTA-1 per nmol of Aβ(1−40) peptide. The binding affinity of 6-OH-BTA-1 to homogenates of frontal cortex from postmortem advanced AD brain also was determined. Again, only a

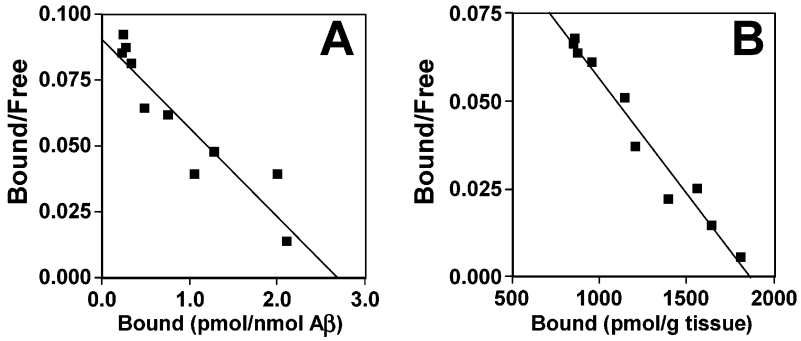

Figure 8. (A) Scatchard plot of the binding of [*N*-methyl-^{3}H]6-OH-BTA-1 to synthetic Aβ(1−40) fibrils. The plot identifies a single binding component with a K_d of 4.7 nM and a B_{max} of 2.7 pmol of 6-OH-BTA-1 bound per nmol of Aβ(1−40). (B) Scatchard plot of the binding of [*N*-methyl-^{3}H]6-OH-BTA-1 to homogenates of frontal cortex from postmortem AD brain. The plot identifies a single binding component with a K_d of 1.4 nM and a B_{max} of 1900 pmol/g tissue (1.9 μM), a value consistent with other assay techniques for Aβ in the frontal cortex of advanced AD subjects.

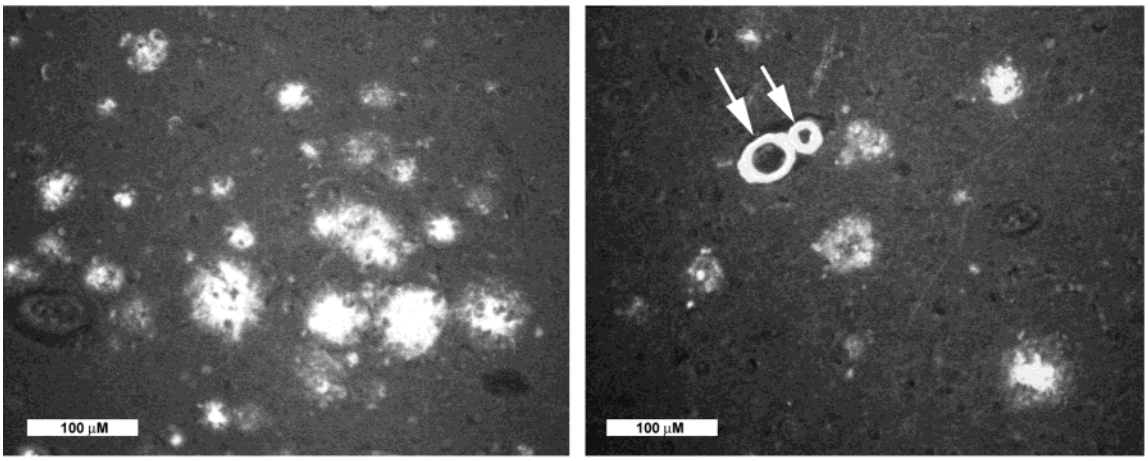

Figure 9. Fluorescence micrographs of sections of AD brain (8 μm thick) stained with 1 μM 6-OH-BTA-1. The section on the left shows numerous compact plaques stained by 6-OH-BTA-1. The section on the right shows several plaques and cross-sections of blood vessels laden with cerebrovascular amyloid, also stained by 6-OH-BTA-1 (marked by arrows).

single binding component was evident, which had a binding affinity (K_d = 1.4 nM) very similar to that observed in Aβ(1−40) fibrils. The B_{max} of 1900 pmol/g tissue (or 1.9 μM) was within the range of 1000−3000 pmol/g total Aβ (1−3 μM) found in AD frontal cortex brain by Naslund and co-workers using biochemical analysis methods.[42] This suggests that the binding stoichiometry of 6-OH-BTA-1 to Aβ in AD brain is close to 1:1 under saturating conditions. It is not clear why the binding stoichiometry of 6-OH-BTA-1 appears to be considerably lower (∼1:370) for synthetic Aβ(1−40) fibrils aggregated in vitro than for homogenates of AD cortical tissue. There was no appreciable specific binding of [*N*-methyl-^{3}H]6-OH-BTA-1 to homogenates of frontal cortex from age-matched control brain (data not shown). In addition, there was no appreciable specific binding of [*N*-methyl-^{3}H]6-OH-BTA-1 to homogenates of cerebellum from age-matched control brain or to homogenates of cerebellum from AD subjects. These findings are in very good agreement with those previously reported for [^{3}H]BTA-1 binding to post-mortem AD and control brain.[43] The absence of [*N*-methyl-^{3}H]6-OH-BTA-1 binding to cerebellar tissues is consistent with histopathological findings in postmortem AD brain that demonstrate the relatively low density of compact Aβ plaques in the cerebellum.[44] This low level of specific binding in the cerebellum makes this region a good candidate for a reference tissue for human PET studies.

Additional experiments were performed using the resources of the NIMH Psychoactive Drug Screening Program to assess whether 6-OH-BTA-1 interacted with any of a representative array of neurotransmitter receptors and transporters.[45,46] The array has been previously reported[45] and includes adrenergic, serotonergic, muscarininc, dopaminergic, opiate, vasopressin, oxytocin, GABA, glutamate, and imidazoline receptor sites. Using 10 μM 6-OH-BTA-1, no inhibition was observed at any receptor site.

As a qualitative measure of specificity for amyloid deposits, nonradiolabeled (cold) 6-OH-BTA-1 was used to stain paraffin sections of postmortem AD brain (Figure 9). Like thioflavin-T, nearly all of the BTA derivatives are fluorescent compounds, and the staining of 6-OH-BTA-1 was localized to both Aβ plaques and cerebrovascular amyloid (CVA) in frontal cortex. The identity of the plaques and CVA stained by 6-OH-BTA-1 was confirmed by staining serial sections with an antibody to Aβ (data not shown). Aβ plaques and CVA are both composed predominantly of Aβ peptides.[47−52] Note the very low background staining of normal brain structures.

The peripheral metabolism of the lead compound [^{11}C]6-OH-BTA-1 in control mice was rapid, with unmetabolized [^{11}C]6-OH-BTA-1 comprising 73 ± 12% of total plasma radioactivity at 2 min after injection and 6.4 ± 2.0% at 30 min. All of the radiolabeled plasma

metabolites of [^{11}C]6-OH-BTA-1 were polar species and were not expected to enter brain. To confirm this, mice were injected with [^{11}C]6-OH-BTA-1, and their brains were removed at 2 and 10 min after injection and homogenized. Radiolabeled species were extracted from the homogenate with ≥94% efficiency using a modified Folch extraction procedure[16] and analyzed using radio-HPLC. Radioactivity in the homogenates was determined to be >95% unmetabolized [^{11}C]6-OH-BTA-1, indicating very low brain entry of radiolabeled metabolites of [^{11}C]6-OH-BTA-1 and little metabolism of the parent compound in brain parenchyma. Attempts to assay the brain concentration of radiolabeled [^{11}C]6-OH-BTA-1 metabolites at 30 min proved unsuccessful as a result of the very low concentration of radioactivity in the mouse brain at this time point (Table 2). The peripheral metabolism of [^{11}C]6-OH-BTA-1 in baboons was similar to that of mice, with unmetabolized [^{11}C]6-OH-BTA-1 comprising 85 ± 3% of total plasma radioactivity at 2 min after injection and 4.3 ± 0.3% after 30 min. The radiolabeled plasma metabolites of [^{11}C]6-OH-BTA-1 in baboon plasma were polar species and displayed similar retention times as the mouse metabolites on reverse phase HPLC analysis.

Discussion

This study was limited to the examination of the properties of a series of 6-substituted 2-(4′-aminophenyl)benzothiazoles. The parent compound of BTA derivatives (thioflavin-T) possesses a 6-methyl substituent, and we have reported the properties of several other 6-substituted BTA's including 6-Me-BTA-0, 6-Me-BTA-1, 6-Me-BTA-2, and BTA-1.[15,16] The studies reported here were intended to more thoroughly explore the effects of 6-position substitution with polar and lipophilic groups on the in vitro and in vivo properties of the BTA derivatives. The syntheses of the precursors and standard 6-substituted BTA derivatives were relatively straightforward, and two different synthetic strategies were employed. Radiolabeling the derivatives with high specific activity [^{11}C]methyl iodide was readily accomplished, although the primary amines provided relatively low radiomethylation yields.

The 18 6-substituted BTA derivatives provided a wide range of log P_{C18} values, varying over nearly 4 orders of magnitude (0.7−4.4) and spanning the log P range of 1−3 predicted for good brain entry. The use of brain concentration (%ID/g) normalized to whole body weight ((%ID-kg)/g) proved useful in comparing the brain penetration of the BTA derivatives across species with body weights varying about 1000-fold. The binding affinities of the BTA derivatives for synthetic Aβ(1−40) ranged from 2 to 64 nM. Conventional wisdom has been that successful PET radioligands should possess K_d (binding dissociation constant) values ≤1 nM. However, it has been pointed out that this requirement could be subject to modification for binding targets that are either in very low or very high concentrations.[53] Another rule of thumb for successful imaging agents is attaining a B_{max}/K_d ratio ≥10, although a lower ratio may be sufficient for PET applications.[54] Given the high concentration of potential Aβ binding sites in AD brain, this would mean a radioligand with a K_d of about 200 nM (2 μM/200 nM = 10) could be sufficient for imaging amyloid in AD. However, it is possible that the concentration of potential Aβ binding sites in very early or presymptomatic AD brain is 1 order of magnitude less than 2 μM and that some of the Aβ binding sites may not be readily accessible to radioligand binding when found in compact cored or neuritic plaques. Thus, compounds with K_d values <20 nM remain potentially attractive as Aβ radioligands until in vivo experiments prove otherwise. This requirement would eliminate only three of the 18 BTA derivatives listed in Table 1.

While the binding affinities of the BTA derivatives were previously reported to be very similar for both Aβ-(1−40) fibrils and frontal cortex from AD brain,[43] the B_{max} values obtained by binding to Aβ fibrils and AD brain homogenates suggested that the stoichiometry of binding was several orders of magnitude different in these two systems. The very low B_{max} value obtained with [*N*-methyl-^{11}C]6-OH-BTA-1 binding to synthetic Aβ fibrils was consistent with the low B_{max} observed with other closely related BTA derivatives such as [*N*-methyl-^{11}C]BTA-1 (unpublished data), and the basis for the low B_{max} value obtained for BTA derivatives with synthetic Aβ fibrils is unknown. One possibility is that in vitro aggregation results in a low percentage of fibrils that accurately mimic those found in AD brain. This could explain the observation that the B_{max} value of BTA derivatives determined in homogenates taken from postmortem AD brain were strikingly higher (~400-fold) than for synthetic Aβ(1−40) fibrils and resulted in a ligand-to-Aβ peptide stoichiometry of about 1-to-1.

The tissue staining findings utilizing nonradiolabeled, fluorescent 6-OH-BTA-1 are similar to those reported for BTA-1.[43] Both amyloid plaques and cerebrovascular amyloid were stained by 6-OH-BTA-1 in a manner similar to serial sections stained with an antibody to Aβ, and relatively little tissue background staining was observed. In a qualitative way, these findings support the specificity of 6-OH-BTA-1 for Aβ deposits, even in the complex milieu of human brain tissue.

The highest control mouse brain entry at early time points was achieved with derivatives possessing log P_{C18} values in the range of 2−3, but the clearance rate of free and nonspecifically bound radioactivity varied inversely with the log P_{C18} values, complicating the identification of the "optimal" radioligand for use as a PET tracer for imaging brain amyloid. Two derivatives, [^{11}C]BTA-1 and [^{11}C]6-OH-BTA-1, clearly demonstrated superior in vivo clearance rates from mouse brain. Baboon brain studies provided qualitatively similar results as the mouse studies, but the clearance rate of the ^{11}C-labeled derivatives was slower from baboon brain. The two lead compounds from the mouse brain studies were also the best compounds in the baboon brain studies, but [^{11}C]6-OH-BTA-1 exhibited free and nonspecifically bound radioactivity clearance properties most similar to other successful PET radioligands. Equally important, [^{11}C]6-OH-BTA-1 exhibited less regional heterogeneity in normal baboon brain when compared to [^{11}C]BTA-1.

Conclusion

The selection of the most promising agent to take forward into human PET imaging studies was made based largely upon the available experimental data

obtained from in vitro binding studies and in vivo studies performed in wild-type mice and normal baboons. The overall encouraging in vitro and in vivo properties of [^{11}C]6-OH-BTA-1 led to the choice of this agent (also referred to as Pittsburgh Compound B or PIB) for further evaluation in human subjects.[55] In vivo studies of both BTA-1[16] and 6-OH-BTA-1[56] have been performed in transgenic mouse models of AD using multiphoton fluorescence microscopy. The one micron resolution afforded by multiphoton microscopic imaging[57] allows the identification of individual amyloid plaques and amyloid-laden cerebral vessels. However, multiphoton fluorescence microscopy requires the administration of compounds at doses >1000-fold higher than those used in PET studies. Nevertheless, the multiphoton approach constitutes an important complement to help interpret PET studies that, by their nature, are performed with spatial resolutions insufficient to distinguish individual plaques. In vivo microPET studies of transgenic mouse models of AD with [^{11}C]6-OH-BTA-1, along with the in vitro and in vivo data described above, may become important points of reference in the development of other amyloid-imaging agents labeled with longer-lived positron-emitting radionuclides, such as 110 min half-life ^{18}F. Such studies are currently being initiated as part of our ongoing program to develop amyloid-imaging compounds.

Experimental Section

General Methods. The syntheses of BTA-0 and BTA-1 (R_6 = H in Figure 1) and 6-Me-BTA-1 (R_6 = Me), and the radiosyntheses of [*N*-methyl-^{11}C]6-Me-BTA-1 and [*N*-methyl-^{11}C]BTA-1 were described previously.[15,16] Compounds 6-Me-BTA-0 and 6-Me-BTA-2 were obtained from Aldrich (Milwaukee, WI). The purities of BTA-0, BTA-1, 6-Me-BTA-0, 6-Me-BTA-1, and 6-Me-BTA-2 were determined using reverse phase and normal phase HPLC (see below), and all five compounds were determined to be greater than 95% pure. Here we report the chemical syntheses of the remaining compounds shown in Figure 1 and the radiolabeling of representative examples of a primary amine ([O-methyl-^{11}C]6-MeO-BTA-0), a secondary amine ([*N*-methyl-^{11}C]6-OH-BTA-1), and a tertiary amine ([*N*-methyl-^{11}C]6-CH_3O-BTA-2) shown in Scheme 2. The reported chemical yields were not optimized.

All commercial reagents and solvents were used without further purification unless otherwise specified. [^{11}C]Methyl iodide was synthesized according to literature methods using the reaction of [^{11}C]carbon dioxide with lithium aluminum hydride followed by hydroiodic acid.[58] High-resolution mass spectra were acquired under electron ionization (EI) conditions using a double-focusing high-resolution mass spectrometer (AUTOSPEC, Micromass Inc.), and samples were introduced by a direct insertion probe. The ^{1}H NMR spectra of all the compounds were recorded on Bruker 300 or 500 MHz spectrometers using tetramethylsilane (TMS) as an internal standard, and chemical shift (δ) data for the proton resonances were reported in parts per million (ppm) relative to internal standard TMS. Elemental analyses of selected compounds were carried out by Midwest Microlab (Indianapolis, IN) or Galbraith Laboratories, Inc. (Knoxville, TN). Thin-layer chromatography (TLC) was performed using Silica Gel 60 F_{254} plates from EM Science and visualized by UV light. Flash chromatography was carried out using Mallinckrodt silica gel 60 (230−400 mesh; column sizes: 54 cm × 2.5 cm, 36.5 cm × 2.5 cm, or 39.2 cm × 2.2 cm) with hexanes and ethyl acetate (EtOAc) as eluents with chromatographic solvent proportions expressed on a volume:volume basis.

Analytical HPLC was performed using either a Phenomenex Prodigy 5 μm ODS(3) 4.6 × 250 mm reverse phase column eluted with an acetonitrile/aqueous buffer (50 mM triethylammonium (TEA) phosphate buffer, pH 7.2) mobile phase mixture or a Phenomenex Silica 5 μm 4.6 × 250 mm normal phase column eluted with an ethyl acetate/hexane/diethylamine (DEA), and both columns were eluted at flow rates of 2.0 mL/min. Both chromatography systems were fitted with a UV detectors (Waters Model 996 set at 350 nm). For detection of radiolabeled compounds, a γ-ray detector (Bioscan Flow-Count fitted with a NaI(Tl) detector) was used in series with the UV detector. Semipreparative HPLC was performed using a Phenomenex Prodigy 10 μm ODS-prep 10 × 250 mm reverse phase column eluted with an acetonitrile/aqueous buffer (50 mM TEA phosphate buffer, pH 7.2) mobile phase mixture, flow rate varied from 5 to 15 mL/min, and UV (Waters Model 481 set at 350 nm) and γ-ray (Bioscan Flow-Count fitted with a PIN detector) detectors. Data acquisition for both the analytical and preparative systems was accomplished using a Waters Millenium Chromatography System.

Synthesis of Precursors and Standard Samples. 2-(4′-(Dimethylamino)phenyl)benzothiazole (BTA-2). A mixture of 2-aminothiophenol (0.5 g, 4.0 mmol), 4-(dimethylamino)-benzoic acid (0.66 g, 4.0 mmol), and polyphosphoric acid (PPA) (10 g) was heated to 220 °C for 4 h. The reaction mixture was cooled to room temperature and poured into 10% potassium carbonate solution (~400 mL). The precipitate was collected by filtration under reduced pressure to give 0.96 g (95%) of the product, which was ca. 90% pure based upon ^{1}H NMR analysis. Recrystallization of 100 mg of the product in methanol gave 80 mg of the pure product. Analytical HPLC: reverse phase (60/40 acetonitrile/triethylammonium (TEA) phosphate buffer pH 7.2) $k' = 7.0$, purity 95.3%; normal phase (10/90/0.2 ethyl acetate/hexane/diethylamine (DEA)) $k' = 2.1$, purity 95.7%. ^{1}H NMR (300 MHz, acetone-d_6) δ: 7.12 (d, $J = 7.7$ Hz, 1 H), 7.01 (d, $J = 9.0$ Hz, 1 H), 6.98 (d, $J = 9.1$ Hz, 2 H), 6.56 (t, $J = 7.8$ Hz, $J = 7.3$ Hz, 1 H), 5.92 (d, $J = 8.9$ Hz, 1 H), 2.50 (s, 6 H). HRMS (EI) *m*/*z* calcd for $C_{15}H_{14}N_2S$ 254.0878, found 254.0879.

Synthesis of 2-(4′-Aminophenyl)-6-methoxybenzothiazole (7; 6-MeO-BTA-0). *N*-(4′-Methoxyphenyl)-4-nitrobenzamide (1). To a solution of anisidine (12.3 g, 0.1 mmol) in pyridine (150 mL) was added 4-nitrobenzoyl chloride (18.5 g, 0.1 mmol). The reaction mixture was heated to reflux for 2 h. Upon cooling to room temperature, the reaction was quenched with water. The precipitate was filtered under reduced pressure. The filtrate was washed with 5% sodium bicarbonate and water and dried at room temperature to give 20.0 g (74%) of *N*-(4′-methoxyphenyl)-4-nitrobenzamide. ^{1}H NMR (300 MHz, DMSO-d_6) δ: 10.47 (s, 1 H, NH), 8.37 (d, $J = 8.5$ Hz, 2 H), 8.18 (d, $J = 8.4$ Hz, 2 H), 7.69 (d, $J = 8.6$ Hz, 2 H), 6.96 (d, $J = 8.4$ Hz, 2 H), 3.77 (s, 3 H).

***N*-(4′-Methoxyphenyl)-4-nitrothiobenzamide (3).** To a solution of *N*-(4′-methoxyphenyl)-4-nitrobenzamide (1) (20.0 g, 73.5 mmol) in chlorobenzene (50 mL) was added Lawesson's reagent (17.8 g, 44 mmol, 0.6 equiv). The reaction mixture was heated to reflux for 3 h. Upon cooling, the products slowly precipitated out from the reaction mixture and filtered under reduced pressure. The filtrate was recrystallized from methanol to give 13.6 g (64%) of *N*-(4′-methoxyphenyl)-4-nitrothiobenzamide. ^{1}H NMR (300 MHz, DMSO-d_6) δ: 8.29 (d, $J = 8.5$ Hz, 2 H), 8.00 (d, $J = 8.4$ Hz, 2 H), 7.76 (d, $J = 8.6$ Hz, 2 H), 7.03 (d, $J = 8.4$ Hz, 2 H), 3.80 (s, 3 H, OCH_3).

2-(4′-Nitrophenyl)-6-methoxybenzothiazole (5). *N*-(4′-Methoxyphenyl)-4-nitrothiobenzamide (**3**) (13.6 g, 47.2 mmol) was first wetted with ethanol (~2 mL), and 30% aqueous sodium hydroxide solution (15 g, 8 equiv) was added. The mixture was diluted with water to provide a final suspension of 10% aqueous sodium hydroxide. Aliquots of this mixture were added at 1 min intervals to a stirred solution of potassium ferricyanide (62 g, 4 equiv) in water (200 mL) at 80−90 °C. The reaction mixture was heated for a further 30 min and then allowed to cool to room temperature. The participate was filtered under reduced pressure and washed with water to give 12.5 g of crude product, which was used in next step without

further purification. ^{1}H NMR (300 MHz, acetone-d_6) δ: 8.36 (m, 4 H), 7.08 (d, J = 8.5 Hz, 1 H), 7.61 (s, 1 H), 7.13 (d, J = 8.5 Hz, 1H), 3.93 (s, 3 H).

2-(4′-Aminophenyl)-6-methoxybenzothiazole (7; 6-MeO-BTA-0). To a solution of 2-(4′-nitrophenyl)-6-methoxybenzothiazole (**5**) (22 mg, 0.077 mmol) in ethanol (10 mL) was added tin(II) chloride dehydrate (132 mg, 0.45 mmol). The reaction mixture was refluxed under nitrogen for 4 h. Ethanol was then evaporated, and the residue was dissolved in ethyl acetate (10 mL). The resulting solution was washed with 1 N sodium hydroxide (2 mL) followed by water (5 mL) and dried over $MgSO_4$. Evaporation of the solvent gave 19 mg (97%) of the product as yellow solid. Analytical HPLC: reverse phase (35/65 acetonitrile/TEA phosphate buffer pH 7.2) k' = 6.2, purity 98.8%; normal phase (50/50/0.2 ethyl acetate/hexane/DEA) k' = 2.1, purity 98.7%. ^{1}H NMR (300 MHz, $CDCl_3$) δ: 7.85 (d, J = 8.7 Hz, 2 H, H-2′ 6′), 7.75 (dd, J_1 = 8.8 Hz, J_2 = 1.3 Hz, 1 H, H-4), 7.31 (d, J = 2.4 Hz, 1 H, H-7), 7.03 (dd, J_1 = 8.8 Hz, J_2 = 2.4 Hz, H-5), 6.56 (d, J = 7.6 Hz, 2 H, H-3′ 5′), 3.84 (s, 3 H, OCH_3). HRMS (EI) m/z calcd for $C_{14}H_{12}N_2OS$ 256.0670, found 256.0679.

Synthesis of 2-(4′-(Methylamino)phenyl)-6-methoxybenzothiazole (18; 6-MeO-BTA-1). 2-Amino-5-methoxythiophenol (15). 2-Amino-6-methoxy-benzothiazole (30.0 g, 172 mmol) was suspended in 50% KOH (180 g KOH dissolved in 180 mL water) and ethylene glycol (40 mL). The suspension was heated to reflux for 48 h. Upon cooling to room temperature, toluene (300 mL) was added and the reaction mixture was neutralized with acetic acid (180 mL). The organic layer was separated, and the aqueous layer was extracted with another 200 mL of toluene. The toluene layers were combined and washed with water and dried over $MgSO_4$. Evaporation of the solvent gave 15.3 g of 2-amino-5-methoxythiophenol as yellow solid. ^{1}H NMR (300 MHz, acetone-d_6) δ: 6.66 (d, J = 2.6 Hz, 1 H), 6.57 (d, J = 8.5 Hz, 1 H), 6.43 (dd, J_1 = 2.6 Hz, J_2 = 8.5 Hz, 1 H), 3.77 (s, 3 H).

2-(4′-(Methylamino)phenyl)-6-methoxybenzothiazole (18; 6-MeO-BTA-1). 4-Methylaminobenzoic acid (11.5 g, 76.2 mmol) and 2-amino-5-methoxythiophenol (**15**) (12.5, g, 80 mmol) were mixed together with PPA (∼30 g) and heated to 170 °C under N_2 atmosphere for 1.5 h. The reaction mixture was cooled to room temperature and poured into 10% K_2CO_3 solution. The precipitate was filtered under reduced pressure. The filtrate was first purified by recrystallization from acetone/water followed by treatment with actived charcoal in THF/water gave 4.6 g (21%) of 2-(4′-methylaminophenyl)-6-methoxybenzothiazole as a yellow solid. Analytical HPLC: reverse phase (35/65 acetonitrile/TEA phosphate buffer pH 7.2) k' = 11.9, purity 98.8%; normal phase (10/90/0.2 ethyl acetate/hexane/DEA) k' = 14.7, purity 98.5%. ^{1}H NMR (300 MHz, acetone-d_6) δ: 7.84 (d, J = 9.0 Hz, 2 H), 7.80 (d, J = 9.0 Hz, 1 H), 7.51 (d, J = 3.0 Hz, 1 H), 7.05 (dd, J_1 = 9.0 Hz, J_2 = 3.0 Hz, 1 H), 6.70 (d, J = 9.0 Hz, 2 H), 3.88 (s, 3 H), 2.85 (d, J = 6.0, 3 H). HRMS (EI) m/z calcd for $C_{15}H_{14}N_2OS$ 270.0827, found 270.0828.

2-(4′-(Dimethylamino)phenyl)-6-methoxybenzothiazole (9; 6-MeO-BTA-2). To a solution of 2-(4′-aminophenyl)-6-methoxybenzothiazole (**7**) (150 mg, 0.59 mmol) in DMSO (anhydrous, 2 mL) were added methyl iodide (297 mg, 2.09 mmol) and K_2CO_3 (500 mg, 3.75 mmol). The reaction mixture was heated at 140 °C for 16 h. Upon cooling to room temperature, the reaction mixture was poured into water and extracted with ethyl acetate (3 × 10 mL). The organic layers were combined, and the solvent was evaporated. The residue was purified by flash column (silica gel, hexanes:ethyl acetate = 9:1) to give 63 mg (38%) of 2-(4′-dimethylaminophenyl)-6-methoxybenzothiazole. Analytical HPLC: reverse phase (60/40 acetonitrile/TEA phosphate buffer pH 7.2) k' = 6.3, purity 99.8%; normal phase (10/90/0.2 ethyl acetate/hexane/DEA) k' = 3.4, purity 95.3%. ^{1}H NMR (300 MHz, acetone-d_6) δ: 7.85 (d, J = 8.9 Hz, 2 H), 7.74 (d, J = 8.8 Hz, 1 H), 7.49 (d, J = 2.4 Hz, 1 H), 7.15 (dd, J_1 = 8.8 Hz, J_2 = 2.4 Hz, 1 H), 6.78 (d, J = 8.9 Hz, 2 H), 3.83 (s, 3 H), 3.01 (s, 6 H). HRMS (EI) m/z calcd for $C_{16}H_{16}N_2OS$ 284.0983, found 284.0985.

2-(4′-Aminophenyl)-6-hydroxybenzothiazole (11; 6-OH-BTA-0). To a suspension of 2-(4′-aminophenyl)-6-methoxybenzothiazole (**7**) (500 mg, 1.95 mmol) in CH_2Cl_2 (20 mL) was injected BBr_3 (1 M in CH_2Cl_2, 5 mL, 5 mmol). The reaction mixture was stirred at room temperature for 16 h and then quenched with 5% HCl. The mixture was neutralized with saturated $NaCO_3$ and extracted with ethyl acetate (6 × 50 mL). The organic layers were combined and washed with water and dried over $MgSO_4$. Evaporation of the solvent gave ca. 500 mg of the crude product, which was purified by flash chromatography (silica gel, hexanes:ethyl acetate = 2:1) to give 360 mg (76%) of 2-(4′-aminophenyl)-6-hydroxybenzothiazole as a solid. Analytical HPLC: reverse phase (35/65 acetonitrile/TEA phosphate buffer pH 7.2) k' = 2.3, purity 99.8%; normal phase (90/10/0.2 ethyl acetate/hexane/DEA) k' = 11.1, purity 99.0%. ^{1}H NMR (300 MHz, Acetone-d_6) δ: 7.86 (s, 1H, OH), 6.95 (d, J = 9.1 Hz, 2H), 6.91(d, J = 8.8 Hz, 1H), 6.55 (d, J = 2.5 Hz, 1 H), 6.17 (dd, J_1 = 8.8 Hz, J_2 = 2.5 Hz, 1 H), 5.95 (d, J = 9.1 Hz, 2 H), 4.45 (s, 2 H, NH_2). HRMS (EI) m/z calcd for $C_{13}H_{10}N_2OS$ 242.0514, found 242.0523.

2-(4′-(Methylamino)phenyl)-6-hydroxybenzothiazole (19; 6-OH-BTA-1). To a suspension of 2-(4′-methylaminophenyl)-6-methoxybenzothiazole (**18**) (3.0 g, 10.4 mmol) in CH_2Cl_2 (100 mL) was injected BBr_3 (1 M in CH_2Cl_2, 35 mL, 35 mmol). The reaction mixture was stirred at room temperature for 16 h. After quenching with water, the reaction mixture was extracted with ethyl acetate (6 × 100 mL). The organic layers were combined, washed with water, and dried over $MgSO_4$. Evaporation of the solvent gave 2.5 g of the crude product, which was purified by flash chromatography (silica gel, hexanes:ethyl acetate = 1:8, followed by THF and MeOH) to give 2.1 g (75%) of 2-(4′-methylaminophenyl)-6-hydroxybenzothiazole. Analytical HPLC: reverse phase (35/65 acetonitrile/TEA phosphate buffer pH 7.2) k' = 7.5, purity 99.6%; normal phase (90/10/0.2 ethyl acetate/hexane/DEA) k' = 10.0, purity 97.9%. ^{1}H NMR (300 MHz, acetone-d_6) δ: 7.88 (d, J = 9.1 Hz, 2 H), 7.73 (d, J = 8.8 Hz, 1 H), 7.38 (d, J = 2.5 Hz, 1 H), 6.99 (dd, J_1 = 8.8 Hz, J_2 = 2.5 Hz, 1 H), 6.83 (d, J = 9.1 Hz, 2 H), 2.83 (d, J = 9.5 Hz, 3 H). HRMS (EI) m/z calcd for $C_{14}H_{12}N_2OS$ 256.0670, found 256.0661. Anal. Calcd for $C_{14}H_{12}N_2OS$: C 65.60; H 4.72; N 10.93; S 12.51. Found: C 65.26; H 5.15; N 10.11; S 11.52.

2-(4′-(Dimethylamino)phenyl)-6-hydroxybenzothiazole (10; 6-OH-BTA-2). To a solution of 2-(4′-dimethyaminophenyl)-6-methoxybenzothiazole (**9**) (3 mg) in CH_2Cl_2 (anhydrous, 3 mL) was added BBr_3 (200 μL, 1.0 M CH_2Cl_2 solution) was injected at −78°C under N_2 atmosphere. The reaction mixture was allowed to warm slowly and stirred at room temperature for another 16 h. After water was added, the reaction mixture was stirred for another 0.5 h. The organic layer was separated, and the aqueous layer was extracted with CH_2Cl_2 (3 × 5 mL). The organic layers were combined and dried with $MgSO_4$. The solvent was evaporated and the residue was purified with preparative TLC to give 1 mg (34%) of 2-(4′-dimethylaminophenyl)-6-hydroxybenzothiazole. Analytical HPLC: reverse phase (35/65 acetonitrile/TEA phosphate buffer pH 7.2) k' = 14.3, purity 99.5%; normal phase (65/35/0.2 ethyl acetate/hexane/DEA) k' = 12.6, purity 98.8%. ^{1}H NMR (300 MHz, DMSO) δ: 9.58 (s, 1 H, OH), 7.85 (d, J = 8.5 Hz, 2 H), 7.71 (d, J = 8.7 Hz, 1 H), 7.33 (s, 1 H), 6.95 (d, J = 8.7 Hz, 1 H), 6.82 (d, J = 8.5 Hz, 2 H), 3.04 (s, 6 H). HRMS (EI) m/z calcd for $C_{15}H_{14}N_2OS$ 270.0827, found 270.0828.

Synthesis of 2-(4′-Aminophenyl)-6-bromobenzothiazole (8; 6-Br-BTA-0). *N*-(4′-Bromophenyl)-4-nitrobenzamide (2). To a solution of 4-bromoaniline (1.0 g, 5.8 mmol) in benzene (20 mL) was added dropwise a solution of 4-nitrobenzoyl chloride (1.08 g, 5.8 mmol) in benzene (20 mL). The reaction mixture was stirred at room temperature for 23 h. The precipitate was filtered under reduced pressure. The filtrate was washed with water thoroughly and recrystallized from ethanol to give 1.6 g (86%) of *N*-(4′-bromophenyl)-4-nitrobenzamide as light yellow solid. ^{1}H NMR (300 MHz,

DMSO-d_6) δ: 10.69 (s, NH), 8.37 (d, J = 8.8 Hz, 2 H), 8.18 (d, J = 8.8 Hz, 2 H), 7.77 (d, J = 8.6 Hz, 2 H), 7.57 (d, J = 8.6 Hz, 2 H).

N-(4′-Bromophenyl)-4-nitrothiobenzamide (4). To a solution of *N*-(4′-bromophenyl)-4-nitrobenzamide (2) (2.8 g, 8.7 mmol) in chlorobenzene (5 mL) was added Lawesson's reagent (2.4 g, 5.9 mmol). The reaction mixture was heated at 120 °C under N_2 atmosphere for 6 h. Upon cooling to room temperature, an orange solid precipitated out from the reaction mixture. The precipitate was filtered and washed with chlorobenzene (1 mL). The filtrate was recrystallized from methanol to give 2.1 g (71%) of *N*-(4′-bromophenyl)-4-nitrothiobenzamide. ^{1}H NMR (300 MHz, DMSO-d_6) δ: 12.18 (s, NH), 8.31 (d, J = 8.5 Hz, 2 H), 8.03 (d, J = 8.5 Hz, 2 H), 7.86 (d, J = 8.6 Hz, 2 H), 7.66 (d, J = 8.6 Hz, 2 H).

2-(4′-Nitrophenyl)-6-bromobenzothiazole (6). *N*-(4′-Bromophenyl)-4-nitro-thiobenzamide (**4**) (1.0 g, 2.97 mmol) was first wetted with ethanol (~0.5 mL), and 30% aqueous sodium hydroxide solution (950 mg 23.8 mmol, 8 equiv) was added. The mixture was diluted with water to provide a final suspension of 10% aqueous sodium hydroxide. Aliquots of this mixture were added at 1 min intervals to a stirred solution of potassium ferricyanide (3.9 g, 11.9 mmol, 4 mol equiv) in water (10 mL) at 80−90 °C. The reaction mixture was heated for another 0.5 h. After cooled to room temperature, the precipitate was filtered under reduced pressure and washed with water. The crude product (0.88 g) was recrystallized from methanol/acetone to give 352 mg (35%) of the 2-(4-nitrophenyl)-6-bromobenzothiazole. ^{1}H NMR (300 MHz, DMSO-d_6) δ: 8.56 (d, J = 1.9 Hz, 1 H), 8.41 (d, J = 8.5 Hz, 2 H), 8.37 (d, J = 8.5 Hz, 2 H), 8.09 (d, J = 8.7 Hz, 1 H), 7.76 (dd, J_1 = 2.0 Hz, J_2 = 8.7 Hz, 1 H).

2-(4′-Aminophenyl)-6-bromobenzothiazole (8; 6-Br-BTA-0). To a solution of 2-(4-nitrophenyl)-6-bromobenzothiazole (32 mg, 0.1 mmol) in ethanol (15 mL) was added tin(II) chloride dehydrate (165 mg, 0.8 mmol). The reaction mixture was refluxed under nitrogen for 1.5 h. After ethanol was evaporated, the residue was dissolved in ethyl acetate (10 mL), washed with 1 N sodium hydroxide (2 mL) and water (5 mL), and dried over $MgSO_4$. Evaporation of the solvent gave a residue, which was purified with preparative TLC (hexanes: ethyl acetate = 70:30) to give 11 mg (38%) of 2-(4′-aminophenyl)-6-bromobenzothiazole as yellow solid. Analytical HPLC: reverse phase (60/40 acetonitrile/TEA phosphate buffer pH 7.2) k' = 4.5, purity 99.2%; normal phase (25/75/0.2 ethyl acetate/hexane/DEA) k' = 9.0, purity 95.3%. ^{1}H NMR (300 MHz, DMSO-d_6) δ: 8.28 (d, J_1 = 1.7 Hz, 1 H), 7.80 (d, J = 8.6 Hz, 1 H), 7.73 (d, J = 8.5 Hz, 2 H), 7.57 (dd, J_1 = 8.6 Hz, J_2 = 1.7 Hz, 1 H), 6.65 (d, J = 8.5 Hz, 2 H), 5.96 (s, 2 H). HRMS (EI) m/z calcd for $C_{13}H_9N_2SBr$ 303.9670, found 303.9665.

2-(4′-(Methylamino)phenyl)-6-bromobenzothiazole (13; 6-Br-BTA-1). To a solution of 2-(4′-aminophenyl)-6-bromobenzothiazole (**8**) (4 mg, 0.013 mmol) in DMSO (anhydrous, 0.5 mL) was added methyl iodide (3.9 mg, 0.027 mmol) and anhydrous K_2CO_3 (100 mg, 0.75 mmol). The reaction mixture was heated at 100 °C for 16 h. Upon cooling to room temperature, the reaction mixture was directly purified by normal phase preparative TLC (hexanes ethyl acetate = 7:3) to give 2.0 mg (50%) of 6-bromo-2-(4′-methylaminophenyl)benzothiazole. Analytical HPLC: reverse phase (60/40 acetonitrile/TEA phosphate buffer pH 7.2) k' = 8.7, purity 99.1%; normal phase (10/90/0.2 ethyl acetate/hexane/DEA) k' = 9.2, purity 96.2%. ^{1}H NMR (300 MHz, acetone-d_6) δ: 8.19 (d, J_1 = 2.0 Hz, 1 H), 7.09 (d, J = 8.8 Hz, 2 H), 7.81 (d, J = 8.8 Hz, 1 H), 7.59 (dd, J_1 = 8.8 Hz, J_2 = 2.0 Hz, 1 H), 6.70 (d, J = 8.8 Hz, 2 H), 5.79 (s, 1 H), 3.17 (s, 3 H).

2-(4′-(Dimethylamino)phenyl)-6-bromobenzothiazole (20; 6-Br-BTA-2). A mixture of 2-amino-5-bromothiophenol (**16**) (204 mg, 1.0 mmol) and 4-(dimethylamino)benzaldehyde (149 mg, 1.0 mmol) in DMSO (1 mL) was heated to 170 °C for 20 min. The reaction mixture was cooled to room temperature and poured into water. The organic component was extracted with ethyl acetate (3 × 10 mL). The combined organic layers were washed with water and dried over $MgSO_4$. Evaporation of the solvent gave a residue that was purified by flash column (hexanes:ethyl acetate = 4:1) to give 179 mg (54%) of the product. Analytical HPLC: reverse phase (60/40 acetonitrile/TEA phosphate buffer pH 7.2) k' = 17.8, purity 99.8%; normal phase (3/97/0.2 ethyl acetate/hexane/DEA) k' = 3.4, purity 99.4%. ^{1}H NMR (300 MHz, acetone-d_6) δ: 8.20 (d, J_1 = 2.0 Hz, 1 H), 7.95 (d, J = 8.8 Hz, 2 H), 7.83 (d, J = 8.8 Hz, 1 H), 7.60 (dd, J_1 = 8.8 Hz, J_2 = 2.0 Hz, 1 H), 6.84 (d, J = 8.8 Hz, 2 H), 3.08 (s, 6H). HRMS (EI) m/z calcd for $C_{15}H_{13}N_2SBr$ 331.9983, found 331.9970.

2-(4′-Aminophenyl)-6-cyanobenzothiazole (12; 6-CN-BTA-0). To a solution of 6-bromo-2-(4′-aminophenyl)benzothiazole (**8**) (27 mg, 0.088 mmol) in 1-methylpyrilidinone (1 mL) was added CuCN (65 mg, 0.71 mmol). The reaction mixture was heat to 200 °C for 18 h. After the mixture was cooled to room temperature, water (5 mL) was added followed by ethylenediamine (0.3 mL). The reaction mixture turned to dark blue and was extracted with ethyl acetate (6 × 10 mL). The organic layers were combined, washed with water, and dried over $MgSO_4$. Evaporation of the solvent afforded a residue, which was purified by preparative TLC (hexanes:ethyl acetate = 2:1) to give 15 mg (68%) of 2-(4′-aminophenyl)-6-cyanobenzothiazole. Analytical HPLC: reverse phase (35/65 acetonitrile/TEA phosphate buffer pH 7.2) k' = 12.0, purity 99.4%; normal phase (50/50/0.2 ethyl acetate/hexane/DEA) k' = 3.0, purity 95.9%. ^{1}H NMR (300 MHz, acetone-d_6) δ: 8.58 (d, J = 1.7 Hz, 1H), 7.98 (d, J = 8.5 Hz, 1 H), 7.82 (dd, J_1 = 1.7 Hz, J_2 = 8.5 Hz, 1 H), 7.79 (d, J = 10.1 Hz, 2 H), 6.65 (d, J = 10.1 Hz, 2 H). HRMS (EI) m/z calcd for $C_{14}H_9N_3S$ 251.0517, found 251.0519.

2-(4′-(Methylamino)phenyl)-6-cyanobenzothiazole (14; 6-CN-BTA-1). To a solution of 2-(4′-methylaminophenyl)-6-bromobenzothiazole (**13**) (54 mg, 0.17 mmol) in 1-methylpyrilidinone (1 mL) was added CuCN (110 mg, 1.4 mmol). The reaction mixture was heat to 170 °C for 17 h. Upon cooling to room temperature, the mixture was diluted with water and the product precipitated out. The precipitate was filtered under reduced pressure and purified by preparative TLC (hexanes: ethyl acetate = 3:2) to give 25 mg (67%) of 6-cyano-2-(4′-methylaminophenyl)benzothiazole. Analytical HPLC: reverse phase (60/40 acetonitrile/TEA phosphate buffer pH 7.2) k' = 3.3, purity 99.2%; normal phase (25/75/0.2 ethyl acetate/hexane/DEA) k' = 4.7, purity 97.5%. ^{1}H NMR (300MH, actetone-d_6) δ: 8.17(d, J = 1.6 Hz, 1 H), 8.04 (d, J = 7.9 Hz, 1 H), 7.96 (d, J = 8.8 Hz, 2 H), 7.70 (dd, J_1 = 1.6 Hz, J_2 = 7.9 Hz, 1 H), 6.68 (d, J = 8.8, 2 H), 2.97 (s, 3 H). HRMS (EI) m/z calcd for $C_{15}H_{11}N_3S$ 265.0674, found 265.0668.

2-(4′-((Dimethylamino))phenyl)-6-cyanobenzothiazole (21; 6-CN-BTA-2). To a solution of 2-amino-5-cyanothiophenol (**17**) (30 mg, 0.5 mmol) in DMSO (1 mL) was added 4-(dimethylamino)benzaldehyde (30 mg, 0.5 mmol). The reaction mixture was heated to 170 °C for 20 min and cooled to room temperature. After it was poured into water, the mixture was extracted with ethyl acetate (3 × 10 mL). The organic layers were combined, washed with water, and dried over $MgSO_4$. Evaporation of the solvent afforded a residue, which was purified by preparative TLC (hexanes:ethyl acetate = 4:1) to give 9 mg (15%) of 2-(4′-dimethylaminophenyl)-6-cyanobenzothiazole. Analytical HPLC: reverse phase (60/40 acetonitrile/TEA phosphate buffer pH 7.2) k' = 7.3, purity 98.7%; normal phase (25/75/0.2 ethyl acetate/hexane/DEA) k' = 1.7, purity 99.3%. ^{1}H NMR (300 MHz, DMSO) δ: 8.85 (d, J = 1.6 Hz, 1 H), 8.41 (s, 4 H), 8.30 (d, J = 8.5 Hz, 1 H), 8.00 (dd, J_1 = 1.6 Hz, J_2 = 8.5 Hz, 1 H), 3.35 (s, 6 H). HRMS (EI) m/z calcd for $C_{16}H_{13}N_3S$ 279.0830, found 279.0822.

Radiosynthesis of Representative 6-Substituted BTA Analogues. [*O*-Methyl-^{11}C]2-(4′-aminophenyl)-6-methoxybenzothiazole ([^{11}C]7; [^{11}C]6-MeO-BTA-0). The radiolabeling precursor, 6-OH-BTA-0 (**11**) (1.0 mg, 4.1 μmoles), was dissolved in 400 μL of DMSO. Dry K_2CO_3 (~5 mg) was added, and the 3 mL V-vial was vortexed for 5 min. No-carrier-added [^{11}C]methyl iodide was bubbled through the solution at 30 mL/min at room temperature. The reaction was heated for 5 min at 95°C using an oil bath. The reaction product was purified

by semipreparative HPLC using an ODS−Prep column eluted with 35/65 acetonitrile/triethylammonium phosphate buffer pH 7.2 (flow at 5 mL/min for 0−13 min, increased to 10 mL/min for 13−18 min, then increased to 15 mL/min for 18−30 min). [*O*-Methyl-^{11}C]6-MeO-BTA-0 eluted at about 24 min. No [*N*-methyl-^{11}C]6-OH-BTA-1 side-product was detected under these reaction conditions. The fraction containing [*O*-methyl-^{11}C]6-MeO-BTA-0 was diluted with 50 mL of water and eluted through a Waters C18 SepPak Plus cartridge. The C18 SepPak was washed with 10 mL of water, and the product was eluted with 1 mL of ethanol (absolute) into a sterile vial followed by 14 mL of saline. Radiochemical and chemical purities were >95% as determined by analytical HPLC ($k' = 6.2$ using the ODS(3) analytical column eluted with 35/65 acetonitrile/triethylammonium phosphate buffer pH 7.2). The radiochemical yield averaged 28.2% at end of synthesis (EOS) based on [^{11}C]methyl iodide, and the specific activity averaged 210 GBq/μmol (5.7 Ci/μmol) at EOS.

[*N*-Methyl-^{11}C]2-(4′-(methylamino)phenyl)-6-hydroxybenzothiazole ([^{11}C]19;[^{11}C]6-OH-BTA-1). 2-(4′-Aminophenyl)-6-methoxymethoxybenzothiazole (24; 6-MOMO-BTA-0). 2-(4′-Nitrophenyl)-6-hydroxybenzothiazole (22). To a suspension of 2-(4′-nitrophenyl)-6-methoxybenzothiazole (**5**) (5.0 g, 18.7 mmol) in CH_2Cl_2 (150 mL) was injected BBr_3 (1 M in CH_2Cl_2, 50 mL, 50 mmol). The reaction mixture was stirred at room temperature for 24 h. The reaction mixture was quenched with water and extracted with ethyl acetate (3 × 100 mL). The extracts were combined and washed with water, dried over $MgSO_4$, and evaporated. The residue was purified by flash column (silica gel, hexanes:ethyl acetate = 4:1) to give 960 mg (20%) of the product as a yellow solid. ^{1}H NMR (300 MHz, acetone-d_6) δ: 9.02 (s, OH), 8.41 (d, J = 9.1 Hz, 1H), 8.33 (d, J = 9.1 Hz, 1H), 7.96 (d, J = 8.6 Hz, 1H), 7.53 (d, J = 2.4 Hz, 1H), 7.15 (dd, J_1 = 8.6 Hz, J_2 = 2.4 Hz, 1H).

2-(4′-Nitrophenyl)-6-methoxymethoxybenzothiazole (23). To a solution of 2-(4′-nitrophenyl)-6-hydroxybenzothiazole (**22**) (960 mg, 3.5 mmol) dissolved in acetone (120 mL, dried over K_2CO_3) was injected methoxymethyl chloride (5 mL) at room temperature. The reaction mixture was monitored with TLC every 30 min, and additional methoxymethyl chloride (ca. 0.5 mL) was added until the reaction was completed. The reaction mixture was then filtered, the mother liquid was concentrated and dried over the high vacuum pump to give 1.0 g of the crude product, which was purified by flash column (hexanes:ethyl acetate = 80:20) to give 833 mg (75%) of the pure product. ^{1}H NMR (300 MHz, acetone-d_6): 8.42 (d, J = 10.9 Hz, 2 H),8.35 (d, J = 10.9 Hz, 2 H), 8.04 (d, J = 9.0 Hz, 1 H), 7.97(d, J = 2.4 Hz, 1 H), 7.30(dd, J_1 = 9.0 Hz, J_2 = 2.4 Hz, 1 H), 5.33 (s, 2 H), 3.49 (s, 3 H).

2-(4′-Aminophenyl)-6-methoxymethoxybenzothiazole (24; 6-MOMO-BTA-0). To a mixture of 2-(4′-nitrophenyl)-6-methoxymethoxybenzothiazole (**23**) (360 mg, 1.14 mmol) and $Cu(OAc)_2$ (207 mg, 1.14 mmol) in anhydrous ethanol (50 mL) was added $NaBH_4$ (866 mg, 22.8 mmol, 20 equiv) while stirring at room temperature. The reaction mixture was stirred for another 1 h. The solvent was then removed under reduced pressure. The residue was dissolved in water and extracted with ethyl acetate (3 × 50 mL). The extracts were combined, dried over $MgSO_4$, and evaporated, and the residue was purified by flash column (hexanes:ethyl acetate = 80:20 to 50:50) to give 306 mg (93%) of the product as a yellow solid. ^{1}H NMR (300 MHz, Acetone-d_6):δ 7.81 (d, J = 8.8 Hz, 3H), 7.64 (d, J = 2.5 Hz, 1H), 7.15 (dd, J_1 = 8.8 Hz, J_2 = 2.5 Hz, 1H), 6.77(d, J = 8.8 Hz, 2H), 5.33 (s, 2H), 3.47 (s, 3H). Anal. Calcd for C 62.92; H 4.93; N 9.78; S 11.20. Found: C 63.03; H 5.26; N 9.43; S 10.85.

[*N*-Methyl-^{11}C]2-(4′-(Methylamino)phenyl)-6-hydroxybenzothiazole ([^{11}C]19;[^{11}C]6-OH-BTA-1). 6-MOMO-BTA-0 (**24**) (1.5 mg, 5.2 μmol) was dissolved in 400 μL of DMSO. Dry KOH (~10 mg) was added, and the 3 mL V-vial was vortexed for 5 min. No-carrier-added [^{11}C]methyl iodide was bubbled through the solution at 30 mL/min at room temperature. The reaction was heated for 5 min at 125° C using an oil bath. A sample of the crude was analyzed by analytical HPLC to determine percent incorporation for [*N*-methyl-^{11}C]6-MOMO-BTA-1 ($k' = 6.6$ for 6-MOMO-BTA-1 on the Prodigy ODS(3) 5 μm analytical column eluted with 50/50 acetonitrile/triethylammonium phosphate buffer pH 7.2). A solution of MeOH/HCl (500 μL, 2/1 MeOH/concentrated HCl) was added to the V-vial, and the reaction was heated an additional 5 min at 125°C. The reaction was neutralized by adding 1 mL of 2.0 M sodium acetate and purified by semipreparative HPLC using a Prodigy ODS−Prep column eluted with 35% acetonitrile/65% triethylammonium phosphate buffer pH 7.2 (flow at 5 mL/min for 0−2 min then increased to 15 mL/min for 2−30 min). [^{11}C]6-HO-BTA-1 eluted at about 11.5 min. The fraction containing [^{11}C]6-OH-BTA-1 was diluted with 50 mL of water and eluted through a Waters C18 SepPak Plus cartridge. The C18 SepPak was washed with 10 mL of water, and the product was eluted with 1 mL of ethanol (absolute) into a sterile vial followed by 14 mL of saline. Radiochemical and chemical purities were >95% as determined by analytical HPLC ($k' = 7.5$ using the Prodigy ODS(3) analytical column eluted with 35/65 acetonitrile/triethylammonium phosphate buffer pH 7.2). The radiochemical yield averaged 12.1% at EOS based on [^{11}C]methyl iodide, and the specific activity averaged 85 GBq/μmol (2.3 Ci/μmol) at EOS.

[*N*-Methyl-^{3}H]2-(4′-(Methylamino)phenyl)-6-hydroxybenzothiazole ([^{3}H]19; [^{3}H]6-OH-BTA-1). The radiosynthesis of [^{3}H]6-OH-BTA-1 was accomplished in a manner similar to that of [^{11}C]6-OH-BTA-1 given above, except that 6.0 GBq of [^{3}H]CH_3I were utilized to radiomethylate 6-MOMO-BTA-0 (2 mg) rather than [^{11}C]CH_3I. The final product was obtained in a 15% radiochemical yield with a radiochemical purity >96% and a specific activity of 2.1 GBq/μmol.

Radiosynthesis of [*N*-Methyl-^{11}C]2-(4′-(Dimethylamino)phenyl)-6-methoxybenzothiazole ([^{11}C]9; [^{11}C]6-MeO-BTA-2). Compound **18** (6-CH_3O-BTA-1) (1.0 mg, 3.7 μmoles) was dissolved in 400 μL of DMSO. Dry KOH (10 mg) was added, and the 3 mL V-vial was vortexed for 5 min. No-carrier-added [^{11}C]methyl iodide was bubbled through the solution at 30 mL/min at room temperature. The reaction was heated for 5 min at 95° C using an oil bath. The reaction product was purified by semipreparative HPLC using a Prodigy ODS−Prep column eluted with 60% acetonitrile/40% triethylammonium phosphate buffer pH 7.2 (flow at 5 mL/min for 0−7 min then increased to 15 mL/min for 7−30 min). The fraction containing [*N*-methyl-^{11}C]6-CH_3O-BTA-2 (at about 15 min) was collected and diluted with 50 mL of water and eluted through a Waters C18 SepPak Plus cartridge. The C18 SepPak was washed with 10 mL of water, and the product was eluted with 1 mL of ethanol (absolute) into a sterile vial followed by 14 mL of saline. Radiochemical and chemical purities were >95% as determined by analytical HPLC ($k' = 4.4$ using the Prodigy ODS(3) analytical column eluted with 65/35 acetonitrile/triethylammonium phosphate buffer pH 7.2). The radiochemical yield averaged 17.3% at EOS based on [^{11}C]methyl iodide, and the specific activity averaged about 160 GBq/μmol (4.3 Ci/μmol) at EOS.

Determination of Octanol−Buffer Partition Coefficients (P_{oct}) and Reverse Phase HPLC Partition Coefficients (P_{C18}). Measurement of the octanol−buffer partition coefficients (P_{oct}) of selected ^{11}C-labeled compounds (Table 1) were performed as previously described.[15] HPLC retention times of all unlabeled (cold) BTA's were determined using reverse phase C18 chromatography [Phenomenex Prodigy ODS(3) 3 μm 4.6 × 250 mm column eluted with 1.4 mL/min acetonitrile/aqueous buffer (60/40 v/v; 50 mM triethylammonium phosphate buffer, pH 7.2)] and UV detection at 365 nm. For example, the retention time (t_R) of BTA-1 under these conditions was 9.98 min and the solvent front appeared at 1.75 min. The retention factor (k'_{C18}) was determined using the equation:

$$k'_{C18} = (t_R - 1.75)/(1.75)$$

From a series of approximately 10 structurally related BTA derivatives (including those of 6-H, 6-CH_3, 6-OCH_3, and 6-OH-

BTA-1 (Table 1)), a correlation of experimentally determined log P_{oct} and log k'_{C18} values was performed resulting in a slope of 2.35, a *y*-intercept of 1.11, and a correlation coefficient of $r = 0.95$. Similar to the method of Salminen and co-workers[59] these values were used in the following equation to determine log P_{C18}, which represents an approximation of the log P_{oct}:

$$\log P_{C18} = 2.35(\log k'_{C18}) + 1.11$$

When limited to compounds with similar structures, this method can yield an accurate representation of relative lipophilicities.[59] In addition, this method avoids the problems encountered in determining log P_{oct} values for compounds having very high or very low lipophilicities and avoids the need to radiolabel each compound.

In Vitro Binding Assays with Aβ(1−40) Fibrils and Brain Homogenates (K_i and K_d determinations). The K_i values of the unlabeled (cold) BTA derivatives for inhibiting [^{3}H]BTA-1 binding to aggregated fibrils of synthetic Aβ(1−40) (BACHEM Bioscience, Inc., King of Prussia, PA) were determined utilizing methods previously reported.[15,16] The aggregation of Aβ(1−40) and the radiosynthesis of [^{3}H]BTA-1 also were previously described.[15,16]

Scatchard analyses were performed to determine the K_d and B_{max} values of [^{11}C]6-OH-BTA-1 ([^{11}C]**19**) for both aggregated fibrils of synthetic Aβ(1−40) and brain tissue homogenates from postmortem medial-frontal cortex gray matter obtained from an autopsy-confirmed AD case through the University of Pittsburgh Alzheimer's Disease Research Center Brain Bank. These Scatchard analyses were performed employing standard methods that have been previously described in detail.[43]

Neuroreceptor Screening. Binding assays for receptors and transporters were performed as previously described using the resources of the National Institute of Mental Health Psychoactive Drug Screening Program.[45,46]

In Vivo Mouse Brain Entry Studies. Studies were performed in female Swiss-Webster mice (23−35 g) in accordance with the Guide for the Care and Use of Laboratory Animals adopted by NIH and with the approval of the local Institutional Animal Care and Use Committee. The mice were injected in a lateral tail vein with 0.37−3.7 MBq (10−100 μCi) of a high specific activity (>7.4 GBq/μmol) ^{11}C-labeled BTA derivative (Table 2) contained in ≤0.10 mL of a solution of 93% isotonic saline and 7% ethanol. The mice were anesthetized and killed by cardiac excision following cardiac puncture to obtain arterial blood samples at 2 or 30 min postinjection. The mouse brains were rapidly excised and divided into cerebellum and remaining whole brain (including brain stem) fractions. The brain samples were counted in a gamma well-counter, and the counts were decay-corrected to the time of injection relative to ^{11}C standards prepared from the injection solution to determine the percent injected dose (%ID) in the samples. The brain samples were weighed to determine the percent injected dose per gram tissue (%ID/g), and this quantity was multiplied by the whole body weight (in kg) to determine the body-weight normalized radioactivity concentration [(%ID-kg)/g] of each tissue sample.

In Vivo Baboon Brain Entry Studies. PET studies were performed in six adult (four female) baboons (*Papio anubis*) (weight 15−35 kg, ages 6−12 years) in accordance with the Guide for the Care and Use of Laboratory Animals adopted by NIH and with the approval of the local Institutional Animal Care and Use Committee. Prior to PET imaging, the animals were initially sedated with ketamine (10−15 mg/kg, im), given atropine (0.5 mg, i.m.) to control salivation and heart rate, and intubated. The baboons were subsequently maintained on a ventilator with isofluorane (0.5−1.25%) anesthesia and medical air. Pancuronium bromide was administered as necessary (iv, up to 0.06 mg/kg/h, titrated to effect) to keep the animals immobilized during the study. A femoral artery catheter was inserted to monitor blood pressure and sample arterial blood, and an intravenous catheter was placed in an antecubital vein for radiotracer injection and to administer fluids as necessary throughout the course of the imaging study. Blood pressure, heart and respiratory rates, and expired CO_2 and oxygen saturation levels were monitored continuously during the PET studies. The baseline rectal body temperature (∼37 °C) was maintained using a heating blanket (Gaymar, Orchard Park, NY) and temperature regulator (Yellow Springs Instruments, Yellow Springs, OH). Prior to scanning, the baboon's head was fixed so that the image planes were acquired approximately parallel to the orbital-meatal line.

PET data were acquired using an ECAT HR+ PET scanner (CTI PET Systems, Knoxville, TN) in 3D imaging mode (63 parallel slices; 15.2 cm axial field-of-view; 4.1 mm full-width half-maximum in-plane resolution). A Neuro-Insert (CTI PET Systems) was used to reduce the contribution of scattered photon events. After the baboons were positioned in the PET scanner, a windowed transmission scan (10−15 min) was obtained for attenuation correction of the PET emission data using rotating ^{68}Ge/^{68}Ga rods. Each of the PET tracers was administered iv over 20 s, and a dynamic series of PET scans were acquired over 60 min using 23 frames of increasing length (6 × 20 s; 4 × 30 s; 6 × 60 s; 4 × 5 min; 3 × 10 min). Approximately 185 MBq (∼5 mCi) of a high specific activity (>14.8 GBq/μmol) ^{11}C-labeled BTA radiotracer was injected in the baboons, including either [*N*-methyl-^{11}C]BTA-1, [*N*-methyl-^{11}C]6-Me-BTA-1, [*N*-methyl-^{11}C]6-OMe-BTA-1 ([^{11}C]**18**), [*N*-methyl-^{11}C]6-CN-BTA-1 ([^{11}C]**14**), or [*N*-methyl-^{11}C]6-OH-BTA-1 ([^{11}C]**19**). In addition in other studies, 148−296 MBq (4−8 mCi) of a high specific activity (>18.5 GBq/μmol) reference PET radiotracer was injected, including either [^{11}C]-raclopride,[60] [^{11}C](+)-McN5652,[39] [carbonyl-^{11}C]WAY100635,[33,34] or [^{18}F]altanserin.[61] The PET data were reconstructed using a Hanning filter (Nyquist cutoff) and corrected for decay, photon attenuation, and scatter.

An MRI scan was obtained for each baboon using a 1.5T GE Signa scanner (GE Medical Systems, Milwaukeee, WI) equipped with a standard head coil. A volumetric spoiled gradient recalled (SPGR) MR sequence with parameters for high contrast among gray matter, white matter, and CSF was acquired in the coronal plane (TE = 5, TR = 24, flip angle = 40°, slice thickness = 1.5 mm, NEX = 2, field of view 12 cm, voxel size = 0.94 × 1.25 × 1.5 mm). Each individual baboon's MR image was coregistered to the PET data using the automated image registration (AIR) algorithm for cross-modality image alignment and reslicing.[62] The initial 16 frames (0−9 min pi) of the dynamic PET images were summed together into images consisting of a single frame. Prior to coregistration, both the MR and summed PET images were edited using the ANALYZE software package (Mayo Clinic, Rochester, MN) to remove extracerebral tissues that could possibly confound the coregistration process. The edited MR images were then coregistered to the summed PET image and resliced to yield MR images in the same spatial orientation and resolution as the summed PET images. The coregistration of MR and PET datasets in the baboon has been demonstrated to be a reliable and robust application of the AIR method.[63,64]

Regions of interest (ROIs) were defined on the coregistered MR image and applied to the dynamic PET datasets to determine regional time−activity data for pons, white matter (cerebral white matter posterior to prefrontal cortex and anterior to lateral ventricles), striatum (caudate and putamen), mesial temporal cortex (amygdala and hippocampus), cerebellum (cerebellar cortex), occipital cortex, and lateral temporal cortex. The ROIs and time-activity curves were created using an internally developed tool based on the interactive data language platform (IDL, Research Systems, Inc., Boulder, CO) and correspond to left and right hemisphere averages (excluding pons). The PET time-activity data were converted to units of microcuries per milliliter using a phantom-based calibration factor and were subsequently normalized to the injected dose and body mass of the animal ((%ID-kg)/g).

Metabolite Determinations of [^{11}C]6-OH-BTA-1 ([^{11}C]-19). Following the injection of [^{11}C]6-OH-BTA-1 ([^{11}C]**19**), arterial whole blood samples were obtained in mice (via cardiac puncture) and baboons (via femoral artery catheter). The

plasma was separated from cellular elements, and the radiolabeled species in the plasma were analyzed as previously described.[16] In addition, the procedures employed to assess radioactivity in the brains of mice 2 and 30 min after injection of about 18.5 MBq (500 μCi) of [^{11}C]6-OH-BTA-1 also have been described.[16]

Tissue Staining. Postmortem brain tissues from autopsy-confirmed AD cases were obtained through the University of Pittsburgh Alzheimer's Disease Research Center Brain Bank. Hippocampus and entorhinal cortex were dissected from 1 cm thick coronal slices. Tissue was processed for staining and quenching of autofluorescence was accomplished according to previously described methods.[12] Quenched tissue sections were taken from PBS into a solution of 1 μM (cold) 6-OH-BTA-1 in PBS pH 7.0 for 45 min. The sections were then dipped for approximately 5 s into water before coverslipping with Fluoromount-G (Electron Microscopy Sciences, Fort Washington, PA). Fluorescent sections were viewed using an Olympus Vanox AH−RFL-LB fluorescence microscope using a UV filter set: U-filter (excites 360−370 nm, dichroic mirror DM400, 420 nm long-pass filter).

Acknowledgment. This work was supported by grants from the National Institute on Aging (AG18402 to C.M. and AG01039 and AG20226 to W.K.), the Alzheimer's Association (IIRG-95-076 and TLL-01-3381 to W.K. and NIRG-00-2355 to Y.W.), and ISOA/AFAR (210304 to Y.W.). Brain tissue for binding and staining assays was provided through the University of Pittsburgh Alzheimer's Disease Research Center Brain Bank (AG05133) by Drs. Steven T. DeKosky and Ronald L. Hamilton. We thank Dr. Bryan Roth of Case Western Reserve University and Dr. Linda Brady of NIMH for allowing us access to the NIMH Psychoactive Drug Screening Program.

References

(1) Braak, H.; Braak, E. Neuropathological stageing of Alzheimer-related changes. *Acta Neuropathol. (Berl.)* **1991,** *82*, 239−259.
(2) Mirra, S. S.; Heyman, A.; McKeel, D.; Sumi, S. M.; Crain, B. J.; Brownlee, L. M.; Vogel, F. S.; Hughes, J. P.; van Bell, G.; Berg, L. The consortium to establish a registry for Alzheimer's disease (CERAD). Part II. Standardization of the neuropathologic assessment of Alzheimer's disease. *Neurology* **1991**, *41*, 479−486.
(3) Klunk, W. E.; Abraham, D. J. Filamentous proteins in Alzheimer's disease: new insights through molecular biology. *Psych. Dev.* **1988**, *6*, 121−152.
(4) Schenk, D. B.; Rydel, R. E.; May, P.; Little, S.; Panetta, J.; Lieberburg, I.; Sinha, S. Therapeutic approaches related to amyloid-beta peptide and Alzheimer's disease. *J. Med. Chem.* **1995**, *38*, 4141−4154.
(5) Schenk, D. B.; Seubert, P.; Lieberburg, I.; Wallace, J. Beta-peptide immunization: a possible new treatment for Alzheimer disease. *Arch. Neurol.* **2000**, *57*, 934−936.
(6) Holtzman, D. M.; Bales, K. R.; Paul, S. M.; DeMattos, R. B. Abeta immunization and anti-Abeta antibodies: potential therapies for the prevention and treatment of Alzheimer's disease. *Adv. Drug Deliv. Rev.* **2002**, *54*, 1603−1613.
(7) Olson, R. E.; Copeland, R. A.; Seiffert, D. Progress towards testing the amyloid hypothesis: inhibitors of APP processing. *Curr. Opin. Drug Discov. Dev.* **2001**, *4*, 390−401.
(8) Matsuoka, Y.; Saito, M.; LaFrancois, J.; Saito, M.; Gaynor, K.; Olm, V.; Wang, L.; Casey, E.; Lu, Y.; Shiratori, C.; Lemere, C.; Duff, K. Novel therapeutic approach for the treatment of Alzheimer's disease by peripheral administration of agents with an affinity for β-amyloid. *J. Neurosci.* **2003**, *23*, 29−33.
(9) Klunk W. E.; Debnath M. L.; Pettegrew J. W. Chrysamine-G binding to Alzheimer and control brain: autopsy study of a new amyloid probe. *Neurobiol. Aging* **1995**, *16*, 541−548.
(10) Mathis C. A.; Mahmood K.; Debnath M. L.; Klunk W. E. Synthesis of a lipophilic radioiodinated ligand with high affinity to amyloid protein in Alzheimer's disease brain tissue. *J. Labelled Compd. Radiopharm.* **1997**, *40*, 94−95.
(11) Dezutter, N. A.; Dom, R. J.; de Groot, T. J.; Bormans, G. M.; Verbruggen, A. M. ^{99m}Tc-MAMA-Chrysamine G, a Probe for beta-Amyloid Protein of Alzheimer's Disease. *Eur. J. Nucl. Med.* **1999**, *26*, 1392−1399.
(12) Styren S. D.; Hamilton R. L.; Styren G. C.; Klunk W. E. X-34, a fluorescent derivative of Congo red: a novel histochemical stain for Alzheimer's disease pathology. *J. Histochem. Cytochem.* **2000**, *48*, 1223−1232.
(13) Klunk W. E.; Bacskai B. J.; Mathis C. A.; Kajdasz S. T.; McLellan M. E.; Frosch M. P.; Debnath M. L.; Holt D. P.; Wang Y.; Hyman B. T. Imaging Abeta plaques in living transgenic mice with multiphoton microscopy and methoxy-X04, a systemically administered Congo red derivative. *J. Neuropathol. Exp. Neurol.* **2002**, *61*, 797−805.
(14) Wang, Y.; Mathis, C. A.; Huang, G.-F.; Holt, D. P.; Debnath, M. L.; Klunk, W. E. Synthesis and C-11-Labeling of (E, E)-1-(3′, 4′-Dihydroxystyryl)-4-(3′-Methoxy-4′-Hydroxystyryl) Benzene for PET Imaging of Amyloid Deposits. *J. Labelled Compd. Radiopharm.* **2002**, *45*, 647−664.
(15) Klunk, W. E.; Wang, Y.; Huang, G.-F.; Debnath, M. L.; Holt, D. P.; Mathis, C. A. Uncharged thioflavin-T derivatives bind to amyloid-beta protein with high affinity and readily enter the brain. *Life Sci.* **2001**, *69*, 1471−1484.
(16) Mathis, C. A.; Bacskai, B. J.; Kajdasz, S. T.; McLellan, M. E.; Frosch, M. P.; Hyman, B. T.; Holt, D. P.; Wang, Y.; Huang, G.-F.; Debnath, M. L.; Klunk, W. E. A lipophilic thioflavin-T derivative for positron emission tomography (PET) imaging of amyloid in brain. *Bioorg. Med. Chem. Lett.* **2002**, *12*, 295−298.
(17) Zhuang Z. P.; Kung M. P.; Hou C.; Plossl K.; Skovronsky D.; Gur T. L.; Trojanowski J. Q.; Lee V. M.; Kung H. F. IBOX (2-(4′-dimethylaminophenyl)-6-iodobenzoxazole): a ligand for imaging amyloid plaques in the brain. *Nucl. Med. Biol.* **2001**, *28*, 887−894.
(18) Zhuang Z. P.; Kung M. P.; Wilson A.; Lee C. W.; Plossl K.; Hou C.; Holtzman D. M.; Kung H. F. Structure−activity relationship of imidazo[1,2-a]pyridines as ligands for detecting beta-amyloid plaques in the brain. *J. Med. Chem.* **2003**, *46*, 237−243.
(19) Agdeppa E. D.; Kepe V.; Liu J.; Flores-Torres S.; Satyamurthy N.; Petric A.; Cole G. M.; Small G. W.; Huang S. C.; Barrio J. R. Binding characteristics of radiofluorinated 6-dialkylamino-2-naphthylethylidene derivatives as positron emission tomography imaging probes for beta-amyloid plaques in Alzheimer's disease. *J. Neurosci.* **2001**, *21*, RC189−.
(20) Shoghi-Jadid, K.; Small, G. W.; Agdeppa, E. D.; Kepe, V.; Ercoli, L. M.; Siddarth, P.; Read, S.; Satyamurthy, N.; Petric, A.; Huang, S. C.; Barrio, J. R. Localization of neurofibrillary tangles and beta-amyloid plaques in the brains of living patients with Alzheimer disease. *Am. J. Geriatr. Psych.* **2002**, *10*, 24−35.
(21) Shi, D. F.; Bradshaw, T. D.; Wrigley, S.; McCall, C. J.; Lelieveld, P.; Fichtner, I.; Stevens, M. F. G. Antitumor Benzothiazoles. 3. Synthesis of 2-(4-aminophenyl)benzothiazoles and evaluation of their activities against breast cancer cell lines in vitro and in vivo. *J. Med. Chem.* **1996**, *39*, 3375−3384.
(22) Kawaoka, Y.; Takashita, K. Preparation of 2-aminothiophenols. Japanese Patent 07278100, 1995.
(23) Tsuruoka, A.; Kaku Y.; Kakinuma H.; Tsukada I.; Yanagisawa M., Nara K., Naito T. Synthesis and antifungal activity of novel thiazole-containing triazole antifungals. II. optically active ER-30346 and its derivatives. *Chem. Pharm. Bull.* **1998**, *46*, 623−630.
(24) Hasebe, N. Use of polyphosphoric acid in the synthesis of 2-arylbenzothiazoles. *Yamagata Daigaku Kiyo, Shizen Kagaku* **1972**, *8*, 63−67.
(25) Dishino, D. D.; Welch, M. J.; Kilbourn, M. R.; Raichle, M. E. Relationship between lipophilicity and brain extraction of C-11-labeled radiopharmaceuticals. *J. Nucl. Med.* **1983**, *24*, 1030−1038.
(26) Vera, D. R.; Eckelman, W. C. Receptor 1980 and Receptor 2000: twenty years of progress in receptor-binding radiotracers. *Nucl. Med. Biol.* **2001**, *28*, 475−476.
(27) Hansch, C.; Leo, A. *Substituent Constants for Correlation Analysis in Chemistry and Biology*; John Wiley and Sons: New York, 1979.
(28) Lemaire, C.; Cantineau, R.; Guillaume, M.; Plenevaux, A.; Christiaens, L. Fluorine-18-altanserin: a radioligand for the study of serotonin receptors with PET: radiolabeling and in vivo biologic behavior in rats. *J. Nucl. Med.* **1991**, *32*, 2266−2272.
(29) Scheffel, U.; Pogun, S.; Stathis, M.; Boja, J. W.; Kuhar, M. J. In vivo labeling of cocaine binding sites on dopamine transporters with [^{3}H]WIN 35,428. *J. Pharmacol. Exp. Ther.* **1991**, *257*, 954−958.
(30) Hume, S. P.; Myers, R.; Bloomfield, P. M.; Opacka-Juffry, J.; Cremer, J. E.; Ahier, R. G.; Luthra, S. K.; Brooks, D. J.; Lammertsma, A. A. Quantitation of carbon-11-labeled raclopride in rat striatum using positron emission tomography. *Synapse* **1992**, *12*, 47−54.
(31) Suehiro, M.; Scheffel, U.; Dannals, R. F.; Ravert, H. T.; Ricaurte, G. A.; Wagner, H. N. Jr. A PET radiotracer for studying serotonin uptake sites: carbon-11-McN-5652Z. *J. Nucl. Med.* **1993**, *34*, 120−127.

(32) Mathis, C. A.; Simpson, N. R.; Mahmood, K.; Kinahan, P. E.; Mintun, M. A. [^{11}C]WAY 100635: a radioligand for imaging 5-HT1A receptors with positron emission tomography. *Life Sci.* **1994**, *55*, PL403−407.

(33) Pike, V. W.; McCarron, J. A.; Lammertsma, A. A.; Osman, S.; Hume, S. P.; Sargent, P. A.; Bench, C. J.; Cliffe, I. A.; Fletcher, A.; Grasby, P. M. Exquisite delineation of 5-HT1A receptors in human brain with PET and [carbonyl-^{11}C]WAY-100635. *Eur. J. Pharmacol.* **1996**, *301*, R5−7.

(34) Drevets, W. C.; Frank, E.; Price, J. C.; Kupfer, D. J.; Holt, D.; Greer, P. J.; Huang, Y.; Gautier, C.; Mathis, C. PET imaging of serotonin 1A receptor binding in depression. *Biol. Psych.* **1999**, *46*, 1375−1387.

(35) Farde, L.; Halldin, C.; Stone-Elander, S.; Sedvall, G. PET Analysis of human dopamine receptor subtypes using ^{11}C−SCH 23390 and ^{11}C-raclopride. *Psychopharmacology (Berl.)* **1987**, *92*, 278−284.

(36) Farde, L.; Pauli, S.; Hall, H.; Eriksson, L.; Halldin, C.; Hogberg, T.; Nilsson, L.; Sjogren, I.; Stone-Elander, S. Stereoselective binding of ^{11}C-raclopride in living human brain-a search for extrastriatal central D2-dopamine receptors by PET. *Psychopharmacology (Berlin)* **1988**, *94*, 471−478.

(37) Smith, G. S.; Price, J. C.; Lopresti, B. J.; Huang, Y.; Holt, D.; Mason, N. S.; Simpson, N. R.; Sweet, R.; Meltzer, C. C.; Sashin, D.; Mathis, C. A. Test-retest variability of serotonin 5-HT2A receptor binding measured with positron emission tomography (PET) and [F-18]altanserin in the human brain. *Synapse* **1998**, *30*, 380−392.

(38) Price, J. C.; Lopresti, B. J.; Mason, N. S.; Holt, D. P.; Meltzer, C. C.; Smith, G. S.; Gunn, R. N.; Huang, Y.; Mathis, C. A. Analyses of [^{18}F]altanserin bolus injection PET data II: consideration of radiolabeled metabolites in humans. *Synapse* **2001**, *41*, 11−21.

(39) Lopresti, B. J.; Mathis, C. A.; Price, J. C.; Villemagne, V. L.; Meltzer, C. C.; Holt, D. P.; Smith, G. S.; Moore, R. Y. Serotonin transporter binding in vivo: further examination of [11C]-McN5652, In *Molecular and Pharmacological Brain Imaging with Positron Emission Tomography;* Gjedde A., Ed.; Academic Press: San Diego, 2001; pp 265−271.

(40) Huang, Y.; Hwang, D. R.; Narendran, R.; Sudo, Y.; Chatterjee, R.; Bae, S. A.; Mawlawi, O.; Kegeles, L. S.; Wilson, A. A.; Kung, H. F.; Laruelle, M. Comparative evaluation in nonhuman primates of five PET radiotracers for imaging the serotonin transporters: [^{11}C]McN 5652, [^{11}C]ADAM, [^{11}C]DASB, [^{11}C]-DAPA, and [^{11}C]AFM. *J. Cereb. Blood Flow Metab.* **2002**, *22*, 1377−1398.

(41) Eckelman, W. C. Sensitivity of New Radiopharmaceuticals. *Nucl. Med. Biol.* **1998**, *25*, 169−173.

(42) Naslund, J.; Haroutunian, V.; Mohs, R.; Davis, K. L.; Davies, P.; Greengard, P.; Buxbaum, J. D. Correlation between elevated levels of amyloid beta-peptide in the brain and cognitive decline. *J. Am. Med. Assoc.* **2000**, *283*, 1571−1577.

(43) Klunk, W. E.; Wang, Y.; Huang, G.-F.; Debnath, M. L.; Holt, D. P.; Shao, L.; Hamilton, R. L.; Ikonomovic, M.; DeKosky, S. T.; Mathis, C. A. The binding of 2-(4′-methylaminophenyl)-benzothiazole to postmortem brain homogenates is dominated by the amyloid component. *J. Neurosci.* **2003**, *23*, 2086−2092.

(44) Wolf, D. S.; Gearing, M.; Snowdon, D. A.; Mori, H.; Markesbery, W. R.; Mirra, S. S. Progression of regional neuropathology in Alzheimer disease and normal elderly: findings from the nun study. *Alzh. Disease Assoc. Disorders* **1999**, *13*, 226−231.

(45) Roth, B. L.; Ernsberger, P.; Steinberg, S. A.; Rao, S.; Rauser, L.; Savage, J.; Hufeisen, S.; Berridge, M. S.; Muzic, R. F. Jr. The in vitro pharmacology of the beta-adrenergic receptor PET ligand (S)-fluorocarazolol reveals high affinity for cloned beta-adrenergic receptors and moderate affinity for the human 5-HT1A receptor. *Psychopharmacology (Berlin)* **2001**, *157*, 111−114.

(46) Rothman, R. B.; Baumann, M. H.; Savage, J. E.; Rauser, L.; McBride, A.; Hufeisen, S. J.; Roth, B. L. Evidence for possible involvement of 5-HT$_{2B}$ receptors in the cardiac valvulopathy associated with fenfluramine and other serotonergic medications. *Circulation* **2000**, *102*, 2836−2841.

(47) Allsop, D.; Landon, M.; Kidd, M.; Lowe, J. S.; Reynolds, G. P.; Gardner, A. Monoclonal antibodies raised against a sub-sequence of senile plaque core protein react with plaque cores, plaque periphery and cerebrovascular amyloid in Alzheimer's disease. *Neurosci. Lett.* **1986**, *68*, 252−256.

(48) Glenner, G. G.; Wong, C. W. Alzheimer's disease: initial report of the purification and characterization of a novel cerebrovascular amyloid protein. *Biochem. Biophys. Res. Commun.* **1984**, *120*, 885−890.

(49) Ikeda, S.; Wong, C. W.; Allsop, D.; Landon, M.; Kidd, M.; Glenner, G. G. Immunogold labeling of cerebrovascular and neuritic plaque amyloid fibrils in Alzheimer's disease with an anti-beta protein monoclonal antibody. *Lab. Investig.* **1987**, *57*, 446−449.

(50) Okamoto, K.; Yamaguchi, H.; Hirai, S.; Shoji, M.; Inoue, K.; Takatama, M. Immunogold electron microscopic study of cerebrovascular and senile plaque amyloid using anti-beta protein antibody. *Prog. Clin. Biol. Res.* **1989**, *317*, 953−963.

(51) Wong, C. W.; Quaranta, V.; Glenner, G. G. Neuritic plaques and cerebrovascular amyloid in Alzheimer disease are antigenically related. *Proc. Natl. Acad. Sci. U. S .A.* **1985**, *82*, 8729−8732.

(52) Yamaguchi, H.; Hirai, S.; Morimatsu, M.; Shoji, M.; Nakazato, Y. Diffuse type of senile plaques in the cerebellum of Alzheimer-type dementia demonstrated by beta protein immunostain. *Acta Neuropathol.* **1989**, *77*, 314−319.

(53) Eckelman, W. C. The use of in vitro models to predict the distribution of receptor binding radiotracers in vivo. *Nucl. Med. Biol.* **1989**, *16*, 233−245.

(54) Eckelman, W. C.; Gibson, R. E. The design of site directed radiopharmaceuticals for use in drug discovery. In *Nuclear Imaging in Drug Discovery, Development and Approval*; Burns, H. D., Gibson, R. E., Dannals, R. F., Siegl P. K. S., Eds.; Birkhauser: Boston, Mass., 1992; pp 113−134.

(55) Engler, H.; Blomqvist, G.; Bergstrom, M.; Langstrom, B.; Klunk, W.; Debnath, M.; Holt, D.; Wang, Y.; Huang, G.-F.; Mathis, C. First human study with a benzothiazole amyloid-imaging agent in Alzheimer's disease and control subjects. *Neurobiol. Aging* **2002**, *23* (Suppl.), S1568.

(56) Hyman, B. T.; Bacskai, B. J.; Kajdasz, S. T.; Mclellan, M. E.; Frosch, M. P.; Debnath, M. L.; Holt, D. P.; Wang, Y.; Mathis, C. A.; Klunk, W. E. Visualizing amyloid plaques. *Neurobiol. Aging* **2002**, *23* (1S), S149.

(57) Bacskai, B. J.; Klunk, W. E.; Mathis, C. A.; Hyman, B. T. Imaging amyloid-beta deposits in vivo. *J. Cereb. Blood Flow Metab.* **2002**, *22*, 1035−1041.

(58) Dannals, R. F.; Ravert, H. T.; Wilson, A. A.; Wagner, H. N. Jr. An improved synthesis of (3-N-[^{11}C]methyl)spiperone. *Int. J. Radiat. Appl. Isot.* **1986**, *37*, 433−434.

(59) Salminen, T.; Pulli, A.; Taskinen, J. Relationship between immobilised artificial membrane chromatographic retention and the brain penetration of structurally diverse drugs. *J. Pharm. Biomed. Anal.* **1997**, *15*, 469−477.

(60) Drevets, W. C.; Price, J. C.; Kupfer, D. J.; Kinahan, P. E.; Lopresti, B.; Holt, D.; Mathis, C. PET measures of amphetamine-induced dopamine release in ventral versus dorsal striatum. *Neuropsychopharmacology* **1999**, *21*, 694−709.

(61) Price, J. C.; Lopresti, B. J.; Mason, N. S.; Holt, D. P.; Huang, Y.; Mathis, C. A. Analyses of [^{18}F]altanserin bolus injection PET data. I: consideration of radiolabeled metabolites in baboons. *Synapse* **2001**, *41*, 1−10.

(62) Woods, R. P.; Mazziotta, J. C.; Cherry, S. R. MRI−PET registration with an automated algorithm. *J. Comput. Assist. Tomogr.* **1993**, *17*, 536−546.

(63) Greer, P. J.; Villemagne, V. L.; Ruszkiewicz, J.; Graves, A. K.; Meltzer, C. C.; Mathis, C. A.; Price, J. C. MR atlas of the baboon brain for functional neuroimaging. *Brain Res. Bull.* **2002**, *58*, 429−438.

(64) Price, J. C.; Drevets, W. C.; Ruszkiewicz, J.; Greer, P. J.; Villemagne, V. L.; Xu, L.; Mazumdar, S.; Cantwell, M.; Mathis, C. A. Sequential $H_2{}^{15}O$ PET studies in baboons: before and after amphetamine. *J. Nucl. Med.* **2002**, *43*, 1090−1100.

JM030026B